PURDUE UNIVERSITY

Graduate School

This is to certify that the thesis prepared

By __Alberto W. Setzer__

Entitled __The Study of Air Pollution Plumes with Imaging Techniques__

Complies with the University regulations and that it meets the accepted standards of the Graduate School with respect to originality and quality

For the degree of:

__Doctor of Philosophy__

Signed by the final examining committee:

_____ , chairman

Approved by the head of school or department:

__Oct. 29__ 19__82__

To the librarian:

This thesis (is not) to be regarded as confidential

Professor in charge of the thesis

THE STUDY OF AIR POLLUTION PLUMES WITH IMAGING TECHNIQUES

A Thesis

Submitted to the Faculty

of

Purdue University

by

Alberto W. Setzer

In Partial Fulfillment of the

Requirements for the Degree

of

Doctor of Philosophy

December 1982

ACKNOWLEDGMENT

TABLE OF CONTENTS

LIST OF TABLES

LIST OF FIGURES

ABSTRACT

Setzer, Alberto W., PhD.   Purdue University, December 1982.
The Study of Air Pollution Plumes With Imaging Techniques.
Major Professor: Robert B. Jacko.

This work examines the possibilities of atmospheric
dispersion studies through the use of small scale images of
air pollution plumes, particularly through the use of
Landsat imagery. The major points are:

1) A historical description of the uses of imaging
techniques in atmospheric and plume dispersion studies.

2) A review of dispersion theories used with smoke and
air pollution photography.

3) A study of a plume (up to 200 km) spreading over the
ocean and visible in Landsat images is developed. Sixteen
cases of this plume indicated that its shape and length
depend mainly on the wind speed.   Long plumes   were
characteristic of winds stronger than 5 m/s and spread
within an angle of 5° to 7.5°.   An association with
Reynolds' (1883) experiments is made in spite of   a
difference of six orders of magnitude between the length of
the plumes in these two works. Pasquill's (1961) horizontal
dispersion coefficients were within an expectd variation

when compared to the values measured from the images. Nevertheless, this variation is associated with limitations in the dispersion equation and in the dispersion coefficients.

4) A study of Landsat multi-spectral data showed that plumes over water have their own spectral signature and that they can be located with an unsupervised classification technique ("Cluster").

5) The remote sensing of plumes is suggested as a viable tool for environmental problems such as acid rain and long-range transport of air pollutants. The use of existing (as well as future) satellite images is a virtually unexplored source of data for environmental studies.

OBJECTIVES

This study examines the application of small scale synoptic images, particularly those of the Landsat satellites, in the analysis of long (10-200 Km range) air pollution plumes from point sources.

The main objective is to examine images of long plumes, together with corresponding meteorological parameters, and determine which parameters are associated with the horizontal dispersion patterns of long plumes. Based on this association, a qualitative model for dispersion of long plumes is to be developed.

A second objective is to determine the applicability of computer mapping of plumes over water and if an unsupervised computer-aided classification technique can be effective to discriminate a plume from a water background.

INTRODUCTION

This work examines the possibilities of atmospheric dispersion studies through the use of small scale images of air pollution plumes, particularly through the use of Landsat imagery (900 km height). Since such images were already collected in reasonable numbers during the last decade in almost every part of the world, and under various meteorological conditions, they constitute a potential data source for pollution studies. As shown, medium range transport of pollutants (from 20 to about 200 km) is easily noticed over bodies of water with clear skies and provides very accessible dispersion data when compared to conventional sampling techniques. Such material can also help theoretical analyses of long range transport of pollution (acid rain, e.g.) by depicting the shape and relative reflectance of long plumes.

Chapter 1 contains a historical description summary of the uses of remote sensing in atmospheric and plume dispersion studies, which is not found in the related literature. It also shows the possibilities of plume photography, ranging from controlled experiments to ocean

crossing dust storms. Particular emphasis is given to satellite photographic studies. No attempt was made to include other remote sensing techniques like radiometric, spectrometric, interferometric and laser analysis of gases and particulates, acoustic radars, etc.

Chapter 2 presents a summary of dispersion theories used with smoke and air pollution photography. A historical perspective is also included.

Chapter 3 describes the case of a plume spreading over the ocean and visible in Landsat images. An association with the experiments of Reynolds (1883) is made, in spite of a difference of six orders of magnitude between the length of the plumes in these two works. A comparison between the horizontal dispersion of the plumes measured from the images and Pasquill (1961) values is also included. A comparison with other long plume data is also included.

Chapter 4 contains a discussion of computer-aided technique to be used with multi-spectral images of air pollution plumes. It is the result of practical work using the methodology available at the Laboratory for Applications of Remote Sensing (LARS), Purdue University.

CHAPTER 1

USES OF IMAGING TECHNIQUES IN ATMOSPHERIC DISPERSION STUDIES

Ground and Aerial Studies

Richardson (1920) was apparently the first to use imaging techniques in the study of atmospheric dispersion. Much earlier drawings and paintings of volcanic eruptions and of smoke from chimneys remain valuable only as a historical account. Richardson (1920) presented three long-exposure photos (60, 75 and 80 s) of paraffin vapor from an extinguished blast-lamp placed 1.9 to 3.4 m above ground level, and up to 10 m downwind. No reference was made to the camera, film or photographic techniques used. The background was the normal vegetation which surrounded the area. This technique was used to test his averaging dispersion theories. For dispersion analysis, aerial photographs of plumes were taken, possibly for the first time, from 1943 to 1945 by Woodcock and Wyman (1945). Oil fog generated by ships in open sea was photographed with vertical (scale in the 1:10,000 range) and oblique photos. Plume lengths were of the order of 1,500 m. again, details of the photogrammetric techniques used were not described in

this reference.

In a military related project, Nelson and Hamsher (1950) used photographs taken from ground level to make a comparative study of films and filters in hte imaging of smoke (and other objects) at altitudes of 4,500 m. Their conclusion (as expected) was that results were improved with long focal-length lenses, high contrast film, and color filters chosen with regard to the spectral relations between object and sky. For unknown reasons, the described technique of and conclusions about enhancing the smoke versus background sky contrast were not considered in subsequent photographic studies of atmospheric dispersion and pollution. Only about thirty years later does this concept seem to have been re-introduced (Veress, 1970, Klauber, 1973, and Setzer et. al., 1982). As a matter of curiosity, dispersion in the atmosphere has been very closely related to military and security problems. In the First World War, about 100,000 people were killed (out of 1,000,300 casualties) by the introduction of gas weapons or by the release of large amounts of gas to downwind targets (U.N., 1969) . With the introduction of atomic weapons in the next war, and to a lesser degree bacteriological weapons a little later, dispersion problems assumed world-wide proportions.

Sartor et al (1952) used 16 mm motion picture cameras to follow variations in shapes of puffs released at different

heights. Film sequences with sky and water background were made using two cameras on a tower. One camera, with a telephoto lens, followed the puff while the other, with a wide angle, photographed large portions of the trajectories. The films were projected over a background with a grid, from which puff growth and trajectory data were obtained. Additional trajectory coordinates were provided by a theodolite with readings synchronyzed with the cameras. Experiments were conducted with puffs which were released by a special device up to about 200 m above the ground, and which lasted a maximum of 20 s.

Another use of filming was reported by Monin (1959), who together with Kasanski, studied size and location of smoke puffs (frequency of 1 frame/5 s) and plumes (1 frame/15 s). In the case of plumes, various frames were combined to obtain average curves for their boundaries. An interesting point made by Monin is that he disagreed that the visible boundary of smoke puffs corresponds to some concentration at which the air becomes opaque. Instead, he claimed that "the concentration beyond the visible smoke puff equals zero." This view was supported by actual sampling. In the discussion of this work, Sutton (Monin, 1959) disagreed with this analysis, and Frenkiel (Monin, 1959) added that "...visible smoke boundaries did not represent lines of constant concentration. These boundaries are probably related to the second derivative of the concentration, but

the relation may be even more complicated."

Much later, the work of Jacko et al. (1978) also presented another use of 16 mm movie cameras. They used two cameras at about 90 degrees in relation to a coke oven in order to obtain the shape of its push plume.

Kellog (1956) presented a study similar to that of Sartor et al., but for stratospheric altitudes. Phototheodolite data from 18 puffs were reduced by computer and by hand work and provided imaging data for a subsequent dispersion study.

A rather careful photogrammetric study of plume spread is found in the work of Clark (1956). Oil fog generated at a 33 m high stack was photographed by two aerial survey cameras 120 m apart and simultaneously shot on the ground at 3.5 s intervals. A three dimensional projector-plotter was built for the analysis in order to compensate for camera tilts, unequal camera-plume distances and plume elevations. Relatively precise contours of the plumes under different meteorological conditions were obtained for further theoretical interpretation. Typical plume lengths depicted in the photos were about 75 m. The authors emphasized the need for good control of the photograph's exposure and processing. They also referred to the problem of different film density that could result from variations in the plume-camera angle in the same pair of photos. Another limitation was the poor contrast between the white smoke and clouds

when using black and white films. This was overcome by using a red colorant in the smoke together with color films. Long exposure pictures (16 exposures at 15 second intervals using contrast panchromatic film) were also obtained, but in this case one of the cameras was directly under the stack and the other 300 m away.

Aerial photography is found again in this period in the work of Hilst (1957; see this same author in chapter 2) but he gave no details about the photographic techniques , except for the flight altitude, 1830 m.

At about this time the literature also registers a photographic study in France, where Saissac (1958) obtained long exposure photos (about 5 minutes) of smoke released at 32 m above the ground. No details about the techniques, or even examples of the pictures, were given.

Davies (1959) had the oportunity to photograph the plume of an oil fire using a helicopter flying up to 3,000 m. Thirty six photographs made it possible to plot the horizontal limits of the plume up to 48 km downwind. The plume dimensions reached up to 3.3 km altitude by 13 km wide and 1.8 km thick.

Culkowski (1961) studied the use of long-time exposure photos for dispersion analysis. Unfortunately, this reference could not be obtained to be used in this thesis. The reader is referred to Gifford (1968) for a pair of

Culkowski's photos showing a 5 min exposure of a plume and the corresponding instantaneous exposure. Many other fine photographs of plumes are also worthy of note in this publication by Gifford.

Halitsky (1961) proposed the use of a single camera and a wind direction recorder that provides the orientation of a plume as a substitute for the more elaborate use of two simultaneous cameras. Halitsky also provided the simple geometry of this technique although he showed no real applications.

Another use of aerial photography is found in the work of Bowne (1961). In this study, plume photos were obtained with a 6 3/8 in. focal-length lens aerial camera in a helicopter flying from 775 m to 1550 m. A K-2 yellow filter was used on clear days, and no filter was used on cloudy days. Photos were taken at thirty-second and one-minute intervals, and maximum plume lengths were about 1500 m.

Hogstrom (1961) developed a method to obtain an integrated image of smoke puffs along the wind direction axis (others were always crosswind) using a 35 mm camera (50 and 135 mm focal-lengths) close to the smoke source. The negatives were projected on white paper, so the contour of the puffs could be drawn for further analysis. The smoke puffs were photographed up to 5,000 m downwind.

A few more aerial studies continued to be made, as in the case of Veress(1970). Vertical photos with 60% overlap from altitudes of 3,000 to 4,500 m and tilted photos (30°) from about 3,000 m were taken using a 70 mm film camera with a 50 mm focal-length lens and Kodak Ektachrome ER-5257 70 mm film. Different combinations of color and Polarizing filters were used. Plumes in the photos were up to about 15 km long.The small scale photos were used with photogrammetric equipment to produce topographic-type maps of the plumes. Polarized photos proved to be the best in depicting plumes as the author expected from theoretical considerations. The most important conclusion was that "the recording, mapping and qualitative analysis of a polluted air mass is possible by photogrammetry" (Veress, 1970).

The conclusions related to this study are fully reported in Veress, 1970a. Since this last reference was not obtained, the following quote from Veress' work was taken from Larsen, 1970. "Using vertical photographs, the horizontal accuracy (of plume measurements) is ±10-20 feet at the source of industrial pollution, decreasing to ±20-50 feet where the concentration of pollutants becomes diluted to about 500 $\mu g/m^3$. Using vertical photographs, the accuracy of elevation is about ±8-19 feet at the source and decreases to ±100-150 feet at about 2 to 2½ miles from the source, where the mass concentration is about 500 $\mu g/m^3$. Using oblique photographs to determine the elevation of the

lower and upper surfaces of the plume cone, accuracies of these elevations were found to be about ±20 feet up to 6 miles from the source where the concentration is approximately 150–200μ/m^3." A stereogram and a topographic map of an air pollution plume from Veress' work is also found in Larsen, 1970.

In a unique air pollution photogrammetric experiment, Veress (1972) compared the optical density of air pollution plumes in the negatives obtained from flights at 6,000 m with actual concentrations obtained by a nephelometer flown through the same plume. The difference between these two techniques under different meteorological conditions was an average of 10%. He also developed an expression relating the photographic and nephelometric measurements. He mentioned many practical limitations in these studies, such as location distortion by lenses, non-linear alterations in recorded luminance due to film characteristics, and development and atmospheric effects. Photos with 60% overlap and also oblique photos from 1,200 m were used in the photogrammetric analysis. Mosaics were also prepared in order to have a full view of the plumes. The best scale for the photos in this study was shown to be 1:120,000.

Klauber (1973) suggested the use of ultraviolet photography with single lens reflex cameras and special lens and interference filters to image sulfur dioxide plumes normally invisible when photographed against the sky. The

sharpness and overall quality of the results are somewhat questionable. No reference was made to the sulfur dioxide concentrations in the photographed plume, leaving open the question of to what extent the results are significant, or just due to different film and film exposure settings. Another application of ultraviolet photos is found in LaBastille and Spiegel (1981) although because of differences in the background it is difficult to compare the normal color and ultraviolet pictures.

A similar concept involving the use of color infrared film and a minus blue filter (yellow) also improved the contrast of coal fired power plant and cooling tower plumes when photographed against blue skies (Setzer, Jacko and Hoffer, 1982). This is only a filtering optical effect and has nothing to do with sky and smoke temperatures as reported, for example, by Hoult et al. (1969). As pointed out earlier in this chapter, the work of Nelson and Hamsher (1950) pioneered this field of applications.

Raynor et al. (1974), made use of aerial photos and their densitometric analysis to determine diffusion coefficients for smoke generated over the sea and spreading towards the shore. A few measurements of actual concentrations were also made. This project was related to plans to install floating nuclear reactors.

Blais (1974) examined photogrammetric techniques that can be used in aerial photos of plumes. His conclusion was that no technique could provide precise data about the location of a tri-dimensional plume. One of the limitations, for example, is that between two consecutive pictures required for a stereoscopic exam there is a time interval in which the plume's spatial configuration changes (Unless the stereo pair is taken simultaneously). Also, a plume is usually opaque, and the location and elevation of a point directly below it has to be geometrically inferred (a process in which the precision depends on the flying height, the position of the nadir point, and the sun elevation). These problems are overcome only by assuming uniform meteorological and dispersion conditions between consecutive photos, a regular geometric cross section of the plume, and by inferring ground characteristics. In the case of non-stereoscopic photos, plume heights can be obtained from the plume shadow and precise information of the camera and sun position. Limitations for this technique will of course involve cloudiness, a sun angle that can cast a visible shadow, and a plume cross section that does not affect its shadow. An error analysis of these three methods was also included (Blais, 1974), and a practical application was made (Hilton and Blais, 1974). This last work also introduced a different idea about the visible edge of plumes. Instead of making the traditional assumption that the plume edge is an isodensity line, the authors stated that the edge is a line

of maximum contrast between plume and background.

High altitude aerial photos of oil fog smoke-generated plumes were obtained from U-2 planes by Nappo (1981; see also Nappo, 1979); ground photos of the same scenes provided additional data. No special care with photogrammetric techniques seemed to be used for evaluating dispersion parameters.

Orbital Studies

But it was the use of images obtained from space that provided a synoptic view of pollution plumes. Two orders of magnitude were added to the length of plumes in dispersion studies - up to 200 km long. Even plumes in another planet were detected (Gifford, et al., 1978), creating the interesting possibility of studying wind and atmospheric patterns in other worlds. And it was only very recently that volcanic plumes were detected on a moon of Jupiter, allowing the comparison of geological processes of other worlds with those of the earth (Morabito et al., 1979, and Smith et al., 1979).

Randerson (1968) discussed photographs taken from Gemini-7 on December, 1965, and Gemini-11 on September,1965, which showed plumes from forest fires, industries, and also haze of industrial origin. A 100 km long and 6.4 Km wide plume originating from forest fires was visible in the Gulf of Florida (see also Anson, 1968, for a color photo, and

Wobber, 1969), and the haze covered an area of 7425 km². industrial origin. Measurements were made taking into account the tilt of the camera axis in relation to the earth surface. This is probably the very first study of plumes and pollution made with data from artificial satellites. Anson (1968) gives details of the equipment used in the Gemini-7 photos of air pollution. A good color photo from Gemini-12 in November, 1966, from 265 km also shows an air pollution plume of industrial nature (Underwood, 1968).

Wobber (1970) reviewed the possibilities of orbital and sub-orbital images as a contribution to a total systems approach to air and water environmental problems. He presented a brief description of the advantages and limitations of pollution studies with Apollo, ERTS (Landsat), Gemini, Mercury, and Viking spacecrafts. Like others, he also recognized the future applications of space surveys in environmental matters. The case of dust movements, with subcontinental proportions, was also quoted. An earlier publication (Wobber, 1969) presented many possibilities and examples of orbital photography in environmental studies.

McLellan (1971) showed that large masses of air with particulate matter could be detected with satellites. He succesfully compared Los Angeles area radiance data from the Applications Technology Satellite III (ATS-III) with visibility and particulates concentration in the atmosphere.

In the range of inter-continental pollution transport, Prospero et al. (1970) showed, with the aid of the ESSA-5 meteorological satellite, how an African dust storm in 1967 crossed the Atlantic Ocean and reached the Caribbean in about 5 days. Due to coarse image resolution only the basic geographic location of the dust cloud could be obtained. A point worth noting in this case is the particle size distribution of the dust obtained by the authors, which showed that on the average most particles were below 10 μ in diameter.

The next step in space study of plumes was the stereographic and photometric analysis presented by Randerson et al. (1971). A 13 km long plume was investigated in the unmanned Apollo-6 pictures obtained with a 70 mm film camera and 76 mm focal length lens. Exposures were made at 8.64 second intervals and Kodak Ektachrome aerial film (SO 121) was used with a Wratten 2E filter. The scale of the imagery varied from 1:2,423,000 to 1:4,022,000 according to variations in orbital altitude from 184 km (perigee) to 306 km (apogee). The ground resolution was estimated at between 23 and 46 m, and the vertical resolution, 100 m. Overlapping ranged from 54 to 72%. Plume geometric characteristics were obtained from photogrammetric relations in individual and stereo pairs of photos. The photogrammetric analysis of plume cross-sections was performed with a four-color isodensitracer and

a microdensitometer.

Skylab (430-km orbit) was the first space program with a pre-determined objective to investigate environmental problems. Because of specific training in this area (Randerson, 1977), the Mission-4 astronauts took 75 photos (out of a total of 2,000) of air pollution cases around the world in 84 days. They registered volcano plumes, brush fires, Saharan dust storms, oil fires, ship trails, pollution palls over cities, etc. Plumes up to 150 km long were visible spreading over the ocean, volcano plumes covered areas of 20,000 km^2, and dust clouds reached 130,000 km^2. Photos were taken mostly with 70 mm cameras, adapted and checked for space use, and the focal length of the lenses varied up to 300 mm. The Skylab photos prepared by Randerson (1977) are probably the best set of space images of air pollution phenomena (see also in the same publication, MacLead et al., 1977, McKee et al., 1977, Friedman and Heiken, 1977, Barnes et al., 1977, Holtz, 1977, Carnegie and Brian, 1977, and Stevenson et al., 1977).

The Russians also made satellite studies of air pollution. Vinogradov et al. (1972) detected dust storms up to 600 km wide over the Gulf of Persia in TV images of ITOS-I. A densitometric analysis of negatives obtained from the TV images was made, and the authors were able to assign four levels of turbidity to the dust clouds. They also noted that turbidity measurements of dust storms could only

be made against dark backgrounds, such as seas, oases, dense vegetation, dark soil or rocks.

Further work was also reported by Grigoryev and Lipatov (1975), who detected agricultural burnings and forest fires in TV images from the Soviet meteorological satellites (Meteor), and also on U.S. ESSA satellite images. Smoke trails about 250 km long were reported along with a smoke cloud with a total amazing length of 5,600 km. An optical densitometric analysis of the plumes of some images was made. The authors also derived a rather simple equation to evaluate the mass of the dust plumes or clouds based on the image recorded density, density of smoke particles, and the "effective radius" of particles.

A very good example of satellite use in air pollution investigation is found in the work of Lyons and his co-workers. They studied plumes on the Chicago-Gary shoreline of Lake Michigan using Landsat imagery and discussed advantages and limitations of this technique. In a series of reports (Lyons, 1973, 1974 and 1975, Lyons and Pease, 1973 and 1973a, and Lyons et al., 1974) they were able to show interesting plume behaviors not yet documented: 100 km long plumes from the Chicago-Gary industrial area crossing Lake Michigan and fumigating over the Michigan state shores, and two remarkable examples showing cumulus clouds which originated partly because of air pollution emissions. The result of a computer-aided technique to enhance Landsat

images, a "clustering" algorithm, (see chapter 4) was also presented, possibly for the first time in association with plumes (Lyons, 1974, and Lyons et al.,1974). These studies also suggested the need for ground truth, which in this case corresponds to plume concentration sampling obtained simultaneously with Landsat images. Copeland et al. (1973) also made a similar proposal involving simultaneous use of Landsat imagery with other remote sensing techniques, air pollution sampling and meteorological information; a densitometric analysis of three plumes in a Landsat image of the Virginia coast was included to show the potential use of these methods. Such results were not found in the literature. Lyons and Pease (1973a) found that band 5 (0.6 to 0.7 μ) showed the sharpest contrast, although theoretical considerations predicted this effect for the near-infrared band 7 (0.8 to 1.1 μ). They also recommended the use of optical densitometry for plume measurements in Landsat pictures. Some of these images have been widely publicized as examples of Landsat capabilities in environment-related problems (Schaefer and Day, 1981 ,LARS, 1977, NASA, 1977).

Landsat satellites, since the launching of the first in the series in July, 1972 (known in the past as Earth Research Technology Satellite - ERTS), have provided more numerous and diversified examples of air pollution detection from space. Images of most land areas around the world have been collected every 18 days for one decade already, thus

providing an immense amount of data. Landsat multispectral data also opened the possibilities for the use of Computer Aided Analysis Techniques in the study of air pollution plumes. Lyons (1974) made use of a "clustering" technique to distinguish plumes over Lake Michigan and Blais et al. (1975) used some LARS functions (see chapter 4) to identify plumes and study their cross-sectional concentrations.

Short et al. (1976) included many remarkable examples of plumes in their book on Landsat images: interaction of plumes and cumulus clouds over Lake Michigan (studied by Lyons and Pease, 1973), agricultural burning in the New Mexico — Texas northern boundary, forest fires in northwest Alaska (see also Torbert, 1976) and in the Northwest territory in Canada, industrial plumes in the Czechoslovakian — Polish border area, burning gas plumes from oil fields in Iraq, emissions from the Titatia volcano in July, 1973, and a curious example of a 560 km long zig-zagging jet contrail over the Gulf of Mexico. An important feature of these Landsat images is that pollution plumes were clearly detected over land areas.

There are also other examples of plumes seen over land. Withington (1976) showed a 46 km long plume which was easily visible over central-northeast Wyoming in December, 1973; the plume originated from gas and oil burning in an oil field fire accident. The narrow spreading of the particulates, about 250 m, and the sharp contrast against

the vegetation are worth noting. Bands 5 and 7 (6 was not shown) best displayed the plume. In a Landsat image of January,1973, Brown and Karm (1976) were able to find steam and fume plumes from power plants on the Ohio River and in the Monongahela River valleys. Four enlarged images of November, 1972, and March, 1973, also showed other plumes near Pittsburgh, PA, and a comparative analysis showed that these smoke plumes are better depicted in band 4. Pettyjohn and McKeon (1976) and Pettyjohn (1980) studied Landsat images showing up to 50 Km long plumes of a ferro-alloy plant and a coal-fired electric generating plant in northeastern Ohio. An image of another area in southeastern Ohio also showed plumes which were suspected of being of man-made origin. Matson (1982) was able to detect a 50 Km long plume over the Amazon forest, and which probably originated from a forest fire or slash burning. The satellite used was the 860 Km altitude polar orbit NOAA-7, in the 0.725-1.1μ and 3.55-3.93μ channels.

In England, Brimblecombe and Davies (1978) presented two Landsat images showing many plumes over land, with the longest one being about 15 km in length. They used surface meteorological charts and sounding data to explain the direction of plume flow. A parallel study (Brimblecombe et al., 1978) focused on the spectral characterization of such plumes. The authors pointed out that the plumes lacked clearly defined boundaries and that edge delineation was a

problem. They also showed, by means of spectral graphs, that plumes and clouds have close spectral characteristics.

In many cases, the Landsat images detect not the plumes themselves, but their effects. Murtha (1973 and 1973a), in a comparative study with aircraft photography, evaluated various levels of long term vegetation damage due to sulfur dioxide emissions, and Wightman (1973) estimated the areas of forest destroyed by fires.

Longer plumes, in the 200 km range, were also found in Landsat imagery, establishing the potential use of remote sensing in studies of long-range transport of air pollutants and in acid rain problems. A 160 km long plume was reported originating from a Copper smelting facility with a 380 m high chimney in Sudbury, Ontario, Canada, in September, 1972, spreading initially over land and then over Lake Huron; the total length of this plume has been estimated at 400 km (Milan and Chung, 1977). Tempelmeyer and Ey (1974) made the analysis of a September, 1972, Landsat image of this plume using the display screen of a digital analyzer. They found the plume to be more clearly visible in the red band (0.6 to 0.7 μ). Distributions of smoke lateral density were also presented, and curiously, were distinct for each spectral band in the same location. A good image of this plume over land was recently published (Maslowski, 1981)

Staylor (1978) investigated theoretical and experimental aspects of the light reflected by plumes and sensed by the Landsat MSS sensors. This seems to be the first time that a quantitative relation was sought between a plume and MSS data. Overlapping, consecutive-day MSS data provided plume and no-plume radiances from an area containing a 6 km long plume. These values from both the plume and its shadow were used to evaluate total particle loading and plume radius, height, particle concentration and scattering functions. The two images were also normalized to correct for minor atmospheric, solar, and viewing-angle changes. Sky radiance was evaluated from cloud shadow data. Effects of sun angle, surface reflectance, signal-to-noise ratio and spatial resolution were also accounted for (Staylor, 1978).

Another long plume, in Cabo Frio, R.J., Brazil, is presented in Chapter 3 of this work. Setzer started to work on this case in 1978, and initial results were soon published (Setzer and Molion, 1979). Torsani (1981), partly supervised by Setzer, proceeded with a study of the initial portion of this plume. A statistical analysis of the plume length and meteorological parameters for 16 different images of the same plume was then made (Setzer, 1981).

And in South Africa, Nijland (1979) was able to identify several 40 Km long industrial plumes over land on Landsat images. In some cases the plume heights were estimated based on the sun elevation at the time the images were

obtained and the distance between the plumes and their shadow.

The various authors in the above-mentioned Landsat cases differed as to which of the various multi-spectral bands made the plumes more visible. From a theoretical and practical point of view, these differences of opinion about the bands should not occur. Chapter 4 provides some insights into this problem.

Geostationary satellites, notwithstanding their 36,000 km distance to the earth's surface, are also able to detect air pollution plumes. Snyder et. al. (1976) showed ATS satellite pictures of a smoke plume in central Florida on May, 1974. Also included in his report were pictures of the same plume obtained by the polar orbit satellites NOAA-3 and DMSP (Defense Meteorological Satellite Program). And Vermillion (1977), in two sucessive passes of the NOAA-5 polar orbit satellite showed how winds picked up dust from New Mexico and wirled it at about 4,500 m over Texas. Lyons and Husar (1976) and Lyons et al. (1978) demonstrated that geostationary satellites can detect large-scale "hazy" air masses associated with sulfate and ozone episodes. Ernst (1975) also showed on a GOES image a haze area an East coast central region. Large Saharan dust storms that reach the Atlantic are also detected by GOES, as in the case of mid-August/82 storm which caused the heaviest dustfall registered over Florida (Jagger, 1982). Matson and Staggs

(1981) presented a GOES thermal infrared image (10.5 to
12.5 μ) showing a plume from Mt. St. Helens (eruption of
18 May, 1980) covering southern Washington, northern and
eastern Idaho, southwestern Montana and Western Wyoming.
See also Danielson (1981) for a more detailed
characterization of Mt. St. Helens' plume. For the
eruptions of the El Chichonal volcano in Mexico (late March
and beginning of April, 1982), GOES images showed that it
took about three weeks for the stratospheric plume to
complete one turn around the globe. The plume was still
noticeable in the images about one month after the eruptions
(Matson, 1982). Setzer noticed that the plume described in
Chapter 3 is sometimes present in the images of GOES
meteorological satellites (visible spectrum), although with
an expected and significant loss in definition when compared
to Landsat images. Jagger (1982) reported that smoke trails
from ships with oil fired boilers are also detected with
GOES. He recalled cases where the trail was more than 1,000
Km long and did not disperse for about five days. Conover
(1966) identified several cloud lines over the ocean with
the shape of plumes often 500 Km long and up to 25 Km wide,
which he suspected of originating from ship emissions. This
hypothesis was later confirmed (Conover, 1969). Among the
causes of the formation of such "ship contrails" Conover
mentioned "1) a convective unsstable layer from the surface
to a low-level stable layer, 2) saturation or slight
supersaturation near the top of the convective layer, and 3)

a convective layer, presumably deficient in cloud forming nuclei" (Conover, 1966). A curious case of GOES use was related by Gird (1982) who showed on an enhanced image the smoke track left by one launching of the Space Shuttle.

Other Techniques

And finally, an example of Side-Looking Airborne Radar (SLAR) use in relation to pollution plumes. However, the objective was to penetrate the plume and "see" the ground surface because the case involved was Mt. St. Helens' eruption on May 18, 1980 (Rosenfeld, 1980). The aircraft used was 10 km west of the peak at an altitude of 8,500 m. X-band, with 3 cm wavelength, penetrated to some extent most of the dense plume. This was the only technique found to monitor lava flows and ground effects of the eruption with such large amounts of smoke. Pictures of the results are included in this reference.

No attempt was made to include in the above summary the subject of remote sensing of averaged air pollution concentrations over large areas in the earth's atmosphere. An initial approach to this field can be found in NASA (1971), Keafer and Kopia (1973), Barringer and Davies (1978), and Ludwig et al. (1974). Nor is there any discussion of Lidar (Lasers) imaging techniques of plumes and acoustic radar equipment. Recent references in this field are Uthe and Wilson, 1979, and Whitaker and Hilst, 1981, for the former, and Thomson, 1975 for the latter.

CHAPTER 2

METHODS OF ANALYSIS

Richardson, in 1920, probably first established the study of atmospheric diffusion through the use of photographs showing the spread of smoke. He developed his own method for evaluating "K", the diffusivity which resulted in the equations previously proposed by Taylor (1915). Richardson's basic equation, (1), can also be used after differentiation, (2), in an almost identical form to Taylor's equations, (3).

$$K = \overline{(h_2 - h_1)^2 / 2(t_2 - t_1)} \qquad (1)$$

$$K = \overline{(h_2 - h_1)Vh} \text{ ,at } t_2 \qquad (2)$$

$$K = \overline{Vh(h - h_0)} = \overline{\tfrac{1}{2}w}(h - h_0) \qquad (3)$$

where:

K = diffusivity, or eddy diffusivity, $[L^2T^{-1}]$.

h_1, h_2 = vertical coordinates of an eddy at time t_1 and t_2, respectively, [L]. For a plume, $(h_2 - h_1)$ is half its width.

t_1, t_2 = time instants, [T].

Vh = vertical velocity of an eddy, $[LT^{-1}]$.

$(h - h_0)$ = "height through which an eddy moves from the layer at which it was at the same temperature as its surroundings, to the layer with which it mixes" (Taylor, 1915), [L].

w = average vertical velocity of the air when it is moving upwards, $[LT^{-1}]$.

_____ horizontal bars correspond to averaged values.

Among the 19 experiments he used to evaluate "K", few involved photos. The three long exposure photos shown cover the spread of smoke over distances of about 6 m and 13 m, with "K" in the vertical direction ranging from 750 to 120 cm^2/s. Plume widths were measured from the eye-drawn contour limits of the plumes.

"K", as used in such atmospheric diffusion studies, corresponds to the same constant found in the so called Fickian diffusion equation (Fick, 1855; see also Csanady, 1973). It is valid also for diffusion of heat in bodies, electricity in conductors, salt in solvents, thermal neutrons in nuclear reactors, etc. Fick's law (see also Einstein, 1905) is stated as:

$$F = -K\nabla X, \text{ and, } \partial X/\partial t = -\nabla \cdot F = \nabla \cdot (K \nabla X), \qquad (4)$$

where:

F = flux, or rate of diffusion, $[ML^{-2}T^{-1}]$.

K = "diffusivity", $[L^2T^{-1}]$.

∇X = gradient of the concentration X, $[ML^{-4}]$.

$\partial X/\partial t$ = partial derivative of the concentration X ($[ML^{-3}]$) with time, $[ML^{-3}T^{-1}]$.

Roberts (1923) was the first to derive a relation between opacity due to smoke clouds and concentration of particulates. His equation for the outline of a Gaussian plume from a continuous point source in an isotropic atmosphere, for example, is:

$$z^2 = 2K\sqrt{x^2+z^2}(\log q^2/4\pi.K.u.N^2-\log\sqrt{x^2+z^2})/\mu \qquad (5)$$

where:

$z,x,$ = coordinates of a point $P(x,y,z)$ in the outline of a plume with its source in the origin, and with wind in the x direction, $[L]$.

K, diffusivity, $[LT^{-2}]$.

μ, mean wind speed along the x direction, $[LT^{-1}]$.

q, emission rate of the point source, $[MT^{-1}]$.

N, "number of particles in a tube of unit cross-section through the observer, necessary to obtain obscuring of background," and where the outline attains a maximum width of $w_i = 2^{1/2}q/\pi^{1/2}e^{1/2}u.N$, independent of K, at a distance $q^2/4\pi KuN^2e = D_1$ from the point of emission and with a total apparent length of $D_2 = e.D_1$ (Roberts,1923).

A first practical application of Robert's equation was tried by Richardson and Proctor (1925) who used data from the eruption in 1920 of a volcano in Japan. The two ash fall patterns reported over land had a D_2/D_1 of about 2, close to the theoretical value of "e". Encouraged by these results they also evaluated "K". The expressions for wi and D_1 were combined in order to eliminate the unknowns q and N, and the result was

$$K = u.w_i^2/8D_1 \qquad (6).$$

Introducing "t_m", the mean time from source to the diameter of maximum width, they found

$$K = \tfrac{1}{2}w_i^2/2t_m \qquad (7)$$

which combined with Equation (1) by Richardson (1920) results in:

$$K = \frac{(\text{standard deviation from mean})}{2(\text{time from source})} = \sigma^2/2t_m \qquad (8).$$

Their conclusion from the above equation was that "...whatever value of the mass-per-area we choose to mark the outline (of the volcano's ash-fall), the half maximum diameter of that outline normal to the mean wind is always the standard deviation at the distance from the source at which it occurs."(Richardson and Proctor, 1925). See also Einstein (1905) for a deduction of this equation, whose practical proof, incidentally, was also done through

photographic studies of diffusion (Seddig, 1908 and 1912, and Henri, 1908a and b).

Another point of this same study is the evaluation of "ϵ", a non-Fickian diffusion parameter that incorporates an increase of K with distance from the source, and whose relation to K was shown to be (Richardson, 1926):

$$\epsilon = K/0.330\sigma^{4/3} \qquad (9).$$

One of the conclusions of Richardson about K was that "no differential equation in which position and time are the independent variables, and mass of diffusing substance per length is the dependent variable, can describe atmospheric diffusion" (Richardson, 1929).

Sutton, after reviewing existing theories of atmospheric turbulent diffusion (Davies and Sutton, 1931), developed his own diffusivity coefficient, "C", a constant value which, by incorporating an increase of eddy size with distance from the source should not vary like K (Sutton, 1932). The plume outline expression deduced from his continuous point source diffusion equation in an isotropic atmosphere is

$$z^2 = C^2 x^m \ln(q/N.\pi^{1/2}C.u.x^{m/2}) \qquad (10)$$

where, in addition to the terms already defined for equation (5):

C = Sutton's diffusion coefficient, $=\sqrt{2\sigma_i/(u.t)^m}$.

m   is an experimental coefficient; m = 2-n, where $(u.\xi)^-$
for n>0 is a function that behaves like $R\xi$, the
correlation coefficient between the motion of the air
for a particle at any instant and the motion for the
same particle after a lapse rate of ξ seconds
(Sutton, 1932). The $R\xi$ concept was first introduced
by Taylor (1922) through purely statistical methods.

σ_1= standard deviation of the particles from their mean
position, [L].

In order to obtain a first estimate of C for continuous
point sources, Sutton proceeded using the limited data of
Richardson (1921) already mentioned. By using a mean value
of K from the works of Richardson and assuming a mean wind
speed, and using a 1.75 value for "m" he obtained analyzing
the data reported by Richardson and Proctor (1925), C at
100m from the source was calculated as 0.6 cm^{18}. According
to his conclusion, this value was comparable with C's found
for balloons spreading over a few hundred kilometers.

Also using photographic techniques, Sutton   measured
dimensions of anti-aircraft shell bursts at heights from
900m to 5400m and, through his plume outline equations,
derived an expression for the variation of C with height
(Sutton, 1932).

A field test of the Fickian versus non-Fickian (where K
varies) dispersion approaches was conducted by Sartor et al.

(1952) while investigating atmospheric eddy diffusion in relation to radar propagation. Smoke puffs from a generator on a tethered balloon not higher than 80m were photographed and filmed up to a maximum of 20 seconds, and the images analyzed with respect to size and time.

The results were much in accordance with Sutton's statistical theory, indicating a variation of K with time, distance and size of the puff. Sutton's equation for the variation of C with height was, however, not confirmed. Details of this experiment and further analyses were presented by Frenkiel and Katz (1956).

Woodcock and Wyman (1947), in what seems to be the first dispersion study using aerial photos, examined plumes generated over open sea. Their method, originated from theories and controlled experiments at the beginning of the century, when extended to the atmosphere assumes small vertical, regular, hexagonal-shapped cells through which the plumes spread. An important point in this approach is that it is used for an instantaneous view of a plume and does not require or assume an averaging profile with time. The cells have the same internal pattern of convectional flow, and the changes in plume direction are due to where it crosses each cell. When shear stresses become significant the vertical cells are replaced by horizontal strips, or double rolls, with axes parallel to the direction of shear. These concepts did explain some of the plume profiles shown;

however, they did not seem useful in developing general equations for plume dispersion.

An optical investigation of growth rates of smoke puffs was also done for stratospheric heights (Kellog, 1956). The data, obtained from 18 puffs and up to a maximum of 11 minutes of dispersion, did not agree with the equations of Sutton and Roberts. A theoretical expression combining some of the principles of Sutton and Roberts, together with Taylor's "diffusion by continuous movement" ,was proposed for the initial seconds of the puffs. No attempt was made to interpret the data in the later stages of the dispersion of the puff due to extreme distortions in the puffs and lack of necessary dimensions of the puffs.

Gifford (1957) introduced a new approach in the analysis of photos of plumes through the use of the similarity theory of relative diffusion. This theory, developed by Brier and Batchelor, establishes that the mean-square puff spreading proceeds as time cubed. Calculations showed this to be reasonably true in the case of the low altitude data of Frenkiel and Katz, but for the stratospheric data of Kellog, no cubed relation was found (Gifford, 1957).

Additional photographic tests of atmospheric dispersion were done by Hilst (1957) through a point source plume in a stable atmosphere, up to 610m downwind. One minute interval pictures taken from about 1770m above the 60m plume level

and a vertical array of impaction samplers provided the dispersion data. The variance (σ^2) of the horizontal displacement of the plume centerline was calculated from the pictures and fitted reasonably well (correlation coefficient of 0.994) the expression $\sigma^2 = a.x^p$, where x is the downwind distance and a, p, constants for specific atmospheric conditions.

Saissac (1958) proposed a variation of the equation developed by Roberts (eq.(5), Chapter 1), in which Ky and Kz, the diffusivities for an anisotropic atmosphere, are substituted by λy and λz, respectively. These new parameters vary with downwind distance, x, according to Ky = $d\lambda$y/dx, and Kz = $d\lambda$z/dx. Very little data seemed to have been obtained by Saissac in order to test his hypothesis. Apparently, no further experiments were made by this author.

In the study of the outlines of plumes, Monin (1959) introduced the use of the Similarity theory of Monin and Obukov. His conclusion was that "the shape of the boundaries of the smoke plume (in particular, their inclination to the horizon) does not depend upon the wind velocity, but does depend upon the stratification of the atmosphere." Also, "the concentration profiles in a smoke plume at different distances from the source are approximately similar to each other. The maximum concentration in the smoke plume is approximately inversely proportional to the distance from the source."

Gifford (1959) deduced a series of simple relations between the average geometry of plumes and dispersion coefficients. He started from the Gaussian averaging diffusion equation in which variances of concentrations were used instead of dispersion coefficients. His formulas for horizontal dispersion are:

$$\nu^2 = u^2 . e(Y_m/X_T)^2 \tag{11}$$

$$\nu^2 = u^2(Y_m/X_m)^2 \tag{12}$$

$$Cy^2 = 2X . \eta . e(Y_m/X_T)^2 \tag{13}$$

$$Cy^2 = 2X_m . \eta(Y_m/X_m)^2 \tag{14}$$

where:

X_T is the total plume length.

Y_m is the maximum plume width.

X_m is the distance of the source to Y_m.

Cy is Sutton's "virtual diffusion coefficient".

η a stability parameter from Sutton's diffusion theory.

ν^2 the Lagrangian turbulence intensities as used, for example by Frenkiel and Katz (1956).

Y_m is half the maximum plume width at a downwind distance X_m.

Also included was the transcendental equation relating the plume half-width Y with the corresponding concentration variance Y^2:

$$Y^2(X/u) = Y^2[\ln(e.Y_m^2/Y^2(X/u))]^{-1} \qquad (15)$$

and which was further used by its author and a co-worker many years later (Gifford, 1981, and Nappo, 1979 and 1981).

The equations of Gifford (1959), Kellog (1956), and Hilst (1957), had another test with (Bowne 1961). Plumes up to about 1km long from a smoke generator at 150ft on a tower were photographed at thirty second or one minute intervals from a helicopter at 2500 to 5000 ft. The results, averaged, seemed inconclusive as far as the fitness of the equations was concerned. Variations between the photographic technique and parallel measurements of turbulence parameters were associated with lack of precision in the photographs and the validity of the models (Bowne, 1961).

A non-Gaussian approach towards the visibility of a plume in a stable atmosphere was deduced by Nonhebel(1960). By assuming that up to about one hundred meters downwind a plume has 95% of its smoke confined to a cone with a horizontal centerline and a semi-angle of 5°, that the observation point is beneath the plume, and that uniform concentration of smoke is found throughout any crosswind section of the plume, he showed that:

$$B = (12.4 \ W/\sigma.u.x')\Sigma(Fr/d) \qquad (16)$$

where:

B = obscuration, percentage of sky light obscured by a

plume section, %. (B = 2.5% was considered the threshold limit of visibility)

W = weight of dust emitted, grains/min.

σ = density of smoke particles, g/cm^3.

u = wind speed, ft/sec.

x' = downwind distance, ft.

Fr = fraction by weight of particles between specified size limits whose average diameter is "d" microns.

The validity of the above equation appeared to be confirmed only through limited observations of a boiler plume which had known size grading (Nonhebel, 1960).

Following the principles laid down by Roberts(1923) and Gifford(1957), Hogstrom(1964) made a photographic study of smoke puffs generated over periods of 30 seconds at different locations (87m, 50m, and 24m above the ground), and emitted during stable conditions. A camera close to the smoke sources photographed the puffs up to 5 km downwind (at regular intervals up to one minute) and produced bidimensional views of the puffs, approximately representing an integration of particulates in the downwind direction. In the 100 experiments conducted, each consisting of a series of puffs which provided average images at fixed distances, an ellipse was fitted to the outline of the

average puff. Hogstrom then calculated the σy's and σx's by measuring the axes of the ellipses and using equations relating these parameters. These equations, which he deduced from the basic Gaussian dispersion equations. are:

$$G_0 = (Q/2\pi.\sigma y.\sigma z)\exp(-a^2/2\sigma y^2) \qquad (17)$$

$$G_0 = (Q/2\pi.\sigma y.\sigma z)\exp(-b^2/2\sigma z^2) \qquad (18)$$

where,

a = a(t) = one of the contour ellipses main axis, [L].

b = b(t) = the second ellipse axis, [L].

G_0 = a constant, related to the integrated concentration along the downwind direction and projected in a plane perpendicular to this direction, [ML^{-2}].

Q = total amount of particulates released, [M].

σy's for one hour sampling time (averaged period of the puffs) was found to be the sum of two parts, one dependent and the other independent of atmospheric stability. Formulae for σz were developed based on stability parameters and surface roughness, and then successfully tested in other experiments described in the literature (Hogstrom, 1964).

Hilton and Blais (1974) presented a different concept in the analysis of aerial photography. They stated that the outline of a plume is defined by a line of maximum contrast between plume and background and not by a line of constant brightness as normally assumed. In this case, the maximum concentration line was parabolic with the apex at the

source, and was given by the formula:

$$\eta = (2Ky.\xi/u)^{12} \qquad\qquad (19)$$

where:

η = lateral half-width of the plume, [L].

Ky = lateral effective diffusion coefficient, $[L^2T^{-1}]$.

ξ = downwind distance along plume axis, [L].

Values for η and ξ were obtained from a least squares fit to a plume outline.

Optical investigation of plumes was made also from space pictures. The first cases were probably those described by Randerson, et al. (1971), who presented a dispersion analysis for an Apollo 6 photograph of an 8 mile long plume taken at 217 km above southern Arizona. The theoretical analysis followed the "Ky" and "Kz" equations summarized by Gifford(1959)-see equations (11) to (14). In addition, an optical densistometric examination revealed a leptokuric distribution of smoke up to 1 km downwind, which changed into a bimodal distribution, instead of the expected Gaussian profiles.

A rather interesting position in the optical analysis of plumes was adopted by Tempelmeyer and Ey (1974), who examined a Landsat image of a 70 km long plume. After an optical densitometric analysis, they refrained from evaluating dispersion parameters by noting that, in general, individual plume shapes do not follow a Gaussian pattern, a

"must" in the above interpretations.

Blais et al. (1975) also developed their model for Landsat multispectral images of plumes. This time they worked with lines of equal brightness on the images and obtained the following solution for Ky:

$$Ky = u.\eta^2/(2\xi_1 \ln(\xi_2/\xi_1))$$ (20)

where the ηs and ξs (as in eq. (19)) are measured in digital displays of the plume.

This author (Setzer and Molion, 1979) used 13 different Landsat images of a 150 km long plume spreading over the ocean to make an approximate evaluation of the plume's dispersion coefficient. A comparison with σy's obtained by Pasquill (1961) indicated that Pasquill's coefficients underestimated the horizontal plume spread by a factor up to about five times. Similar conclusions were also presented by Torsani (1981), who limited his study of this same plume to a range of 20 km. Torsani's conclusion about the factors that govern the plume spread was that the dispersion can be related mainly to temperature differences between the ocean and the air.

Another approach for this plume was also proposed by Setzer (1981). Simple regression equations were fitted to plume length and various meteorological parameters. The best correlation found was between the plume length and wind speed. The following two equations best fit the data:

$$Xt = 58.4 \; lnv + 10.8 \qquad (r^2 = 0.87) \qquad\qquad (21)$$

$$Xt = 12.8 \; v + 31.4 \qquad (r^2 = 0.75) \qquad\qquad (22)$$

where:

Xt is the visible length of the plume, km.

v is the wind speed, m/s.

The limits of wind speed that can be used in this equation are a function of the sampling population, i.e., between 1.0 and 12.0 m/s.

Another way to look at equation (22) is that it indicates a constant ratio between the wind speed and the plume length, or, a constant time that the plume remains visible. This constant time is the value of the inverse of the tangent of the curve, 3.6 hours.

CHAPTER 3

A NOVEL APPROACH TO DISPERSION OF LONG PLUMES

Stating the Problem

Picture 3.1 shows the subject of this chapter: a 140 km long air pollution plume recorded over the ocean by a Landsat satellite. But let us start with some questions related to what we are actually examining, from both the remote sensing and dispersion point of views.

First, how much information does this picture, from about 917 km above the surface, provide?

The imaging device of Landsat is a multispectral scanner (MSS) with picture elements (pixels) corresponding to a ground area of about 79 m by 57 m (NASA,1976). This does not mean that smaller objects cannot be detected. Even the reflection of sunlight from a small mirror placed on an area covered with vegetation has been recorded by Landsat (Evans, 1974). In this case, the pixel that covered the area containing the mirror (4,500 m^2) showed a higher average ground reflectance than its surrounding pixels.

The higher light reflectance of the smoke in comparison to that of the water results in correspondingly higher values for the smoke pixels. These values represent averages of the smoke reflectance when the plume is opaque, or of the smoke and water combined when the plume is semi-opaque. Provided the MSS detects the smoke, the ground resolution of about 80 m corresponds to an imprecision of 16% in the 0.5 km range, 0.008% in the 100 km range, and so forth. These percentages are significant for crosswind plume dimensions, although they can be neglected for the length of long plumes. Another point that has to be considered is that the reflectance differences of water and smoke are small, which also imposes limitations on the problem of defining the plume outline - see Table 4.1, in next chapter.

These considerations indicate that minor changes in atmospheric turbidity, as well as in the wave and color patterns of the water surface, can cause enough variations in the light reflected by the plume and the sea so that any precise location of the plume contour is precluded.

As noted in the previous chapter, different researchers as well as this author reported differing bands to be adequate for plume detection over water. It seems possible now to understand these discrepancies. Still water reflects very little solar light in band 7 (0.8-1.1μ), and since the particulates in the smoke do reflect in this range, one could theoretically expect this band to provide the best
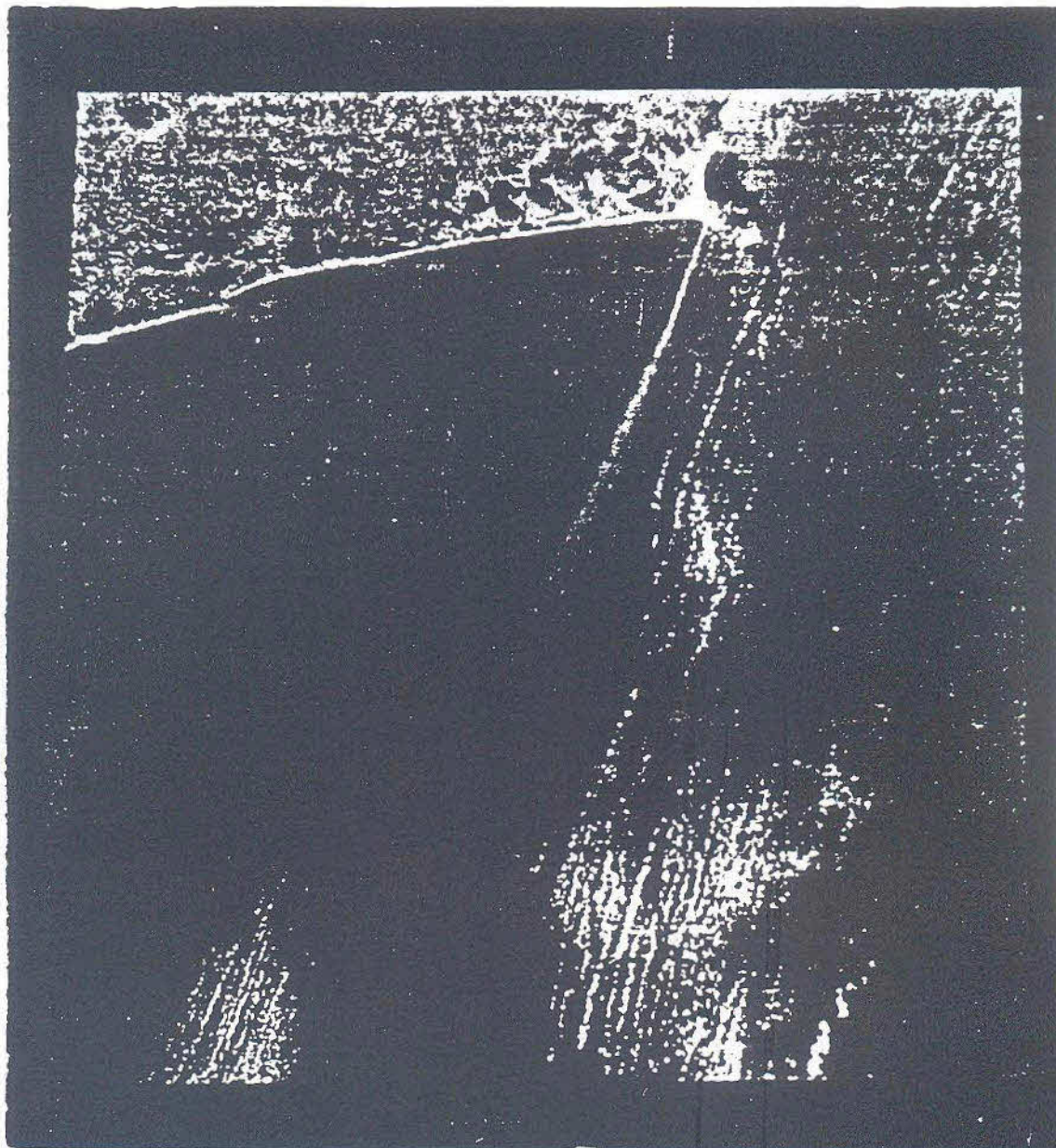
Figure 3.1. 140 Km long plume spreading over the ocean. The wind was 8 m/s, from NE; the temperature gradient was about $-5.6^{\circ}C/Km$. The air was $9.5^{\circ}C$ warmer than the sea. Landsat image of March/07/76, 11:38 GMT, 38° solar elevation. The plume originates at about $22^{\circ}59'S$ and $42^{\circ}02'W$.

recordings. However, if dispersion conditions cause the plume to become diluted in the atmosphere, the band 7 sensor also penetrates the plume more efficiently. Penetration in the near-IR bands is a recorded fact - see Pease and Bowden, 1969. Figure 3.2 shows such spreading conditions. Also, good dispersion conditions are normally associated with strong winds, which in turn cause more waves on the water surface, which themselves cause higher reflectance to the MSS sensors. Band 4 ($.5-.6\mu$), on the other extreme of the MSS spectrum, records more light from the water surface when compared to other bands, thus reducing the distinction between plumes and water. Again, water roughness and dispersion conditions can also affect the capability of the MSS sensors in this range.

Thus, we can see that any tentative efforts to equate plume detection with respect to such natural environmental variations will be highly difficult, if at all possible. Such considerations also impose limitations on a calibration involving simultaneous satellite imaging and plume concentration sampling.

The experience gathered from the case presented in this and the following chapter indicates that two steps have to be followed to examine plumes in Landsat imagery:

a) All spectral bands have to be checked for the best plume image.

b) Plumes in all spectral bands are better detected in a visual display unit through "stretching" the image (an enhancing technique), or by examining digital printouts which indicate the energy levels of the pixels.

The second important question is:

Is this a plume which will fit commonly used dispersion theories ?

As seen in Chapter 2, almost all dispersion theories assume average plume shape and concentration over a period of time. The reason for this statistical approach can be traced back to Richardson (1926) when he questioned, "Does the wind possess a velocity ?"; his own answer, based on the definition that velocity = $\Delta x/\Delta t$ for $\Delta t \to 0$, was in the negative.

In this case, we are looking at an almost instantaneous view of the plume. The ground speed of the MSS Landsat swaths is about 5,800 m/s, thus requiring an interval of 25s between the recording of the extremes of a 140 km long plume like the one in Figure 3.1. Since the smoke takes a few hours to travel this distance (8 m/s wind for Figure 3.1), the difference between these two time scales is three orders of magnitude. Therefore, for practical purposes the Landsat images are instantaneous views of the plumes.

The widely used Pasquill-Hay-Gifford dispersion curves
and equations (Turner, 1969, for example) were based on
average data for distances up to one kilometer downwind and
were obtained during intervals of a few minutes. This
theory also assumes that the dispersion is inversely
proportional to the wind speed (Pasquill, 1961). Most
imaging dispersion analyses quoted in Chapter 2 also follow
these principles. These averaging approaches, as shown
below, do not provide an interpretation for instantaneous
views of plumes. Also, it was found that the inverse effect
of the wind speed on long plumes is questionable. And among
the non-averaging techniques, none was found adequate for
images of long plumes.

Therefore, the limitations of the Landsat remote sensing
system and also the inadequacy of existing dispersion
theories made it necessary to develop a novel approach to
analyze long plumes.

Assumptions

A few assumptions and considerations about the long plume
under study were made before the dispersion analysis.

a) Background and plume reflectance conditions for each
image are constant. This means, for each image, that no
significant variations in atmospheric turbidity or sea
reflectance characteristics occur along the plume.

b) The emission rate of the stack is constant. This assumption is made based on information provided by the industry that emitted the plume (Alcalis, 1979). It will be one of the working bases for the dispersion model derived below.

c) The visibility of a plume depends on the number and size of its particles (or gas molecules, or both) which are in the area covered by a pixel and which reflect sunlight back to space. This number is assumed to be a function of the pollutant concentration in the plume and of the dimensions of the plume. Therefore, a plume becomes invisible when the smoke particles on a pixel decrease to a certain number which could reflect enough light to sensitize the MSS sensor. This limit number apparently varies with the atmosphere transparency, background (water) reflectance characteristics and sun angle.

d) The plumes do not necessarily have a Gaussian concentration profile. Figure 3.3 shows this condition for a relatively short plume and Figures 3.4 and 3.5 for a long plume. Even plumes such as the one in Figure 3.1 could not be classified with certainty as Gaussian. If we should imagine the plume of Figure 3.1 inside a cone or tube, the concentration in any of its cross sections could also be considered as uniform, as seen from Landsat. Another example of this is found in jet contrails in the upper layers of the troposphere. If under clear skies we observe

contrails for some time, we notice that they seem to keep
some uniformity of concentration as they disperse. We do
not see the contrails better defined at their center when
they are close to their visibility threshold. Instead, they
become invisible almost homogeneously along any cross
section. Gaussian profiles for plumes are obtained when the
sampling is made at fixed positions over a period of time;
the variation of concentrations at each point is also
Gaussian (see Millan, 1976, for an interesting point of view
about the geometry of plumes).

A Novel Approach

The starting point for this novel approach in the
photogrammetric analysis of long plumes is that the total
visible length of a plume and its shape are a measure of the
atmospheric dispersion characteristics. The assumption of
the same pollution rate for differing images is essential
for the comparison of the various plume lengths. If, for
example, the emission rate is very low, the plume may not be
visible at all, or became invisible within a close range of
the stack. No assumptions are required in order to examine
the shape of plumes because even a small portion of their
length seems to provide the desired information.

The hypothesis drawn from this length and shape approach
is that the dispersion characteristics of long plumes seem
to be governed mainly by the wind speed. This is probably

Figure 3.2. A plume showing wide spreading.4.6 m/s NE wind; the temperature gradient was about =5.3°C/Km. The air was 11°C warmer than the sea. Case 9.

Figure 3.3. A non-Gaussian plume. West wind or 1.1 m/s; The air was 2°C warmer than the sea water. Landsat image of May/22/77; solar elevation of 30°. Image processed by Torsani(1981) and not included on Table 3.1.
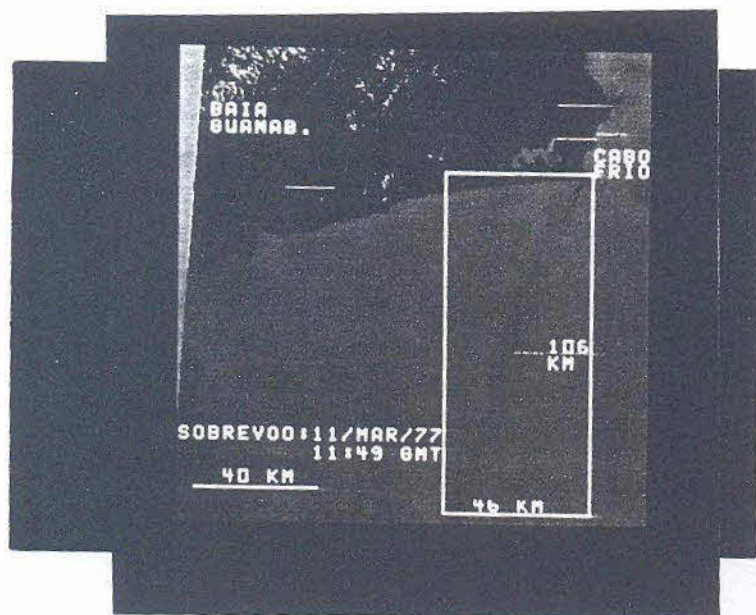
Figure 3.4. A segmented long plume with an 8.5m/s NE wind and temperature gradient of -5.8°C/Km. The air was 7°C warmer than the sea; solar elevation of 38°. Case 15.

Figure 3.5. Digital enlargement of Figure 3.4.
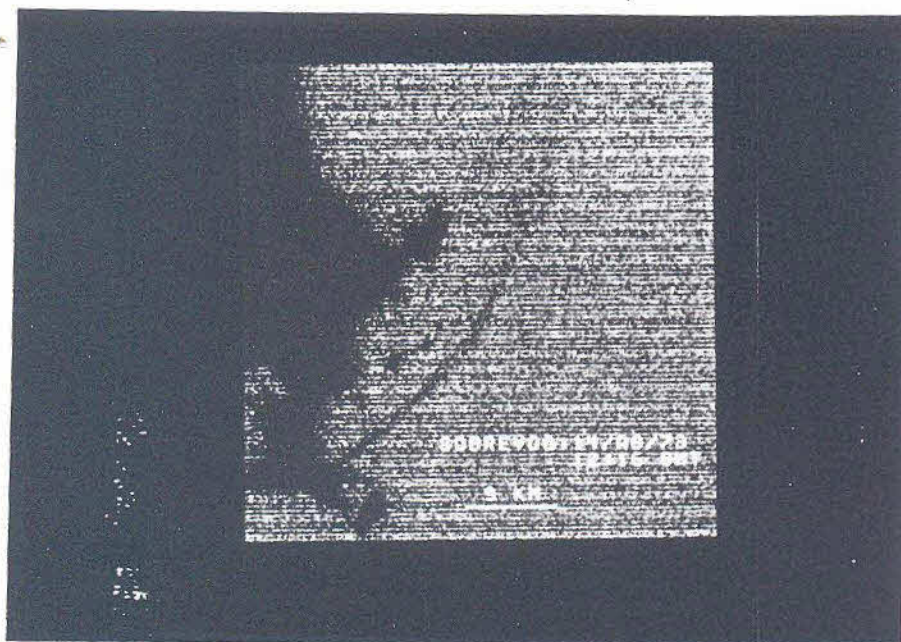
Figure 3.6. A curved plume with a 7 m/s SW wind. Landsat image of Sept./19/73, 12:15 GMT. Case 2.

Figure 3.7. An oscillating plume. Case 16.

true also for plumes over land and not only over open sea as in this case.

Evidence

The evidence for the foregoing conclusion is found upon examination of 16 different images of the same plume.

Data Sources. The plume is emitted by an Alkalai complex located on the shoreline of Cabo Frio, state of Rio de Janeiro, Brazil, some 120 km east of the city of Rio de Janeiro. The emission parameters of the main stack, as provided by the factory (Alkalis, 1979) are: chimney height, 76 m; gas flow rate, 200 m^3/s; exit gas speed, 7 m/s; gas average composition by volume: 47% of water vapor, 41% of nitrogen, 10% of oxygen, 2% of carbon dioxide, and traces of CO, NOx, SO_2, Mg, ClS, $MgSO_4$, NaCl. The exactiness of these data could not be verified, and the unusual high water vapor content (if correct) could be an indication of condensation of the plume in a saturated atmosphere (all the other gases are transparent, and the "traces" of other substances shouldn't be so clearly visible for 150 Km.

Satellite images used were those obtained through the ERTS/Landsat program. During the period studied, 1973-1977, 16 images were selected for analysis. Other images showed excessive cloud cover or bad recording of data; some were not available at the archives. The images are available as Compatible Computer Tapes (CCTs) at INPE (1979) and were

processed with INPEs automatic analyzer GE-IMAGE 100 (G.E.,
1975). Each of the images used had its plume versus ocean
contrast enhanced by a different combination of Landsat
bands and enhancing programs since no particular pattern was
found useful to all images. The enhanced images displayed
on the equipment's video were photographed for subsequent
enlargement. The plume dimensions shown on these
enlargements were then measured with a conventional ruler.

Meteorological data used for the analysis were obtained
from a government-operated station (M.A., 1973-78) very
close to the factory, with records at 08:00, 14:00 and 20:00
hours, local time. High altitude data were obtained from
the international airport at Rio de Janeiro (FAB, 1975-78).
The soundings were scheduled for 08:00 local time and were
always within ½ hour of the time the satellite pictures were
taken. See Table 3.2 for a summary of the data.

Data Interpretation

After examining 16 different images of this plume (see
Table 3.2) it was clear that its shape changed in each
satellite image and that its cross sections were not
necessarily Gaussian. These characteristics were considered
an indication that the plume flow was of a turbulent nature.
It was also noted that limitations associated with the
satellite sensing system did not provide enough details of
the plume to allow an accurate measure of its dimensions in

crosswind directions. Therefore, a method of interpretation was used that would require as few assumptions as possible regarding the dispersion patterns. The parameters chosen for this purpose were the length and the shape of the plume. This approach, to a certain extent, is similar to the one adopted by Reynolds in the study of laminar and turbulent flows (Reynolds, 1883). Although the causes of the change from laminar to turbulent flow were largely unknown to Reynolds he devised a non-dimensional number that indicated the kind of flow to be expected: the well-known $Re=\rho vD/\mu$. In this case, the plume is seen as resembling the dye Reynolds introduced to the flow of water inside a tube. The behavior of the plume is considered an indication of the flow characteristics and therefore of the dispersion conditions. The length relation, however, between Reynolds' experiment and this plume is 10^6 ! Another difference is that fewer parameters can be used in these plume cases than in the general problem that Reynolds solved. There are no significant variations in density or viscosity of the fluids (air and plume), and the flow is not confined. If so, the plume behavior should be mainly a function of wind speed.

One may think that this approach is restricted by the effect of temperature differences between the surface and the air, and between different layers of air in the lower atmosphere. However, this seems not to be the case. Thermal mixing (convection) in the lower atmosphere seems to

occur with weak winds, and it tends to be reduced with strong winds. Therefore, it also depends on the wind speed. Table 3.1 shows the correlation coefficients for plume length and various meteorological parameters. Plume length shows higher correlation with wind speed ($r^2=0.87$) than with any other meteorological variable — an indication that supports the foregoing explanation.

Figure 3.8 shows the plume length as a function of the wind speed for the cases used in Table 3.2. Long plumes of more than 90 km occurred with winds stronger than 5 m/s, and up to 12 m/s. Shorter plumes, up to 45 km, were characteristic of lighter winds, although one case (No.2) of 7 m/s was reported. Altitude data was not available for this last case, and one cannot be sure about its meaning. In another case, No.10, altitude data showed that after a few dozen meters the wind speed decreased. If this were also true for case No.2, then it would not be an exception. Other correlations in Table 3.1 are high, and they must be examined carefully. For example, the gradients of potential and normal temperature show an r^2 of 0.78. Such a high value is actually expected since potential temperatures are calculated from normal temperatures. The instantaneous σy at 40 Km from the source showed a high correlation with the plume length. The problem in this case is that short plumes did not even reach 40 Km and, therefore, the high correlation is just an (obvious) indication that long plumes

Table 3.1. Correlation coefficients for plume length and meteorological parameters.

	w.d. 10m	w.v. 10m.	w.v. alt.	r.h. 10m	r.h. alt.	Δw 10m	Δt/Δz	Δθ/Δz	σy 20Km	σy 40Km
Plume length	-0.55	0.50	0.87	-0.43	0.05	-0.24	-0.12	-0.13	-0.01	0.82
Wind speed, 10m	-	-	0.19	0.14	-0.07	-0.17	0.42	0.44	0.05	0.48
Wind speed, alt.	-	-	-	-0.35	0.20	-0.07	-0.34	-0.06	-0.10	0.52
Rel. Humid., 10m	-	-	-	-	-0.54	-0.06	0.81	0.75	-0.21	0.61
Rel. Humid.,alt.	-	-	-	-	-	-0.13	-0.28	-0.03	0.48	-0.08
Wind variation in 24 hs, 10m	-	-	-	-	-	-	-0.49	-0.61	-0.62	-0.71
Δtemp./Δaltit.	-	-	-	-	-	-	-	0.78	-0.31	0.06
Δθpoten./altit.	-	-	-	-	-	-	-	-	0.16	0.48
σy at 20Km	-	-	-	-	-	-	-	-	-	0.74

"alt." corresponds to altitude data(see Table 3.2).

Curve Fitting(10m and altitude data)

1. $L = a.v + b$

(1) $L = 6.72.v + 47.95$ $(r^2=0.25)$

(2) $L = 12.81.v_a + 31.38$ $(r^2=0.75)$

2. $L = a.e^{b.v}$

(3) $L = 45.69.e^{0.0855.v}$ $(r^2=0.22)$

(4) $L = 37.06.e^{0.1634.v_a}$ $(r^2=0.64)$

3. $L = a + b.lnv$

(5) $L = 50.96 + 23.6.lnv$ $(r^2=0.15)$

(6) $L = 10.83 + 58.4.lnv_a$ $(r^2=0.77)$

4. $L = a.v^b$

(7) $L = 48.8.v^{0.28}$ $(r^2=0.12)$

(8) $L = 27.93.v^{0.76}$ $(r^2=0.68)$
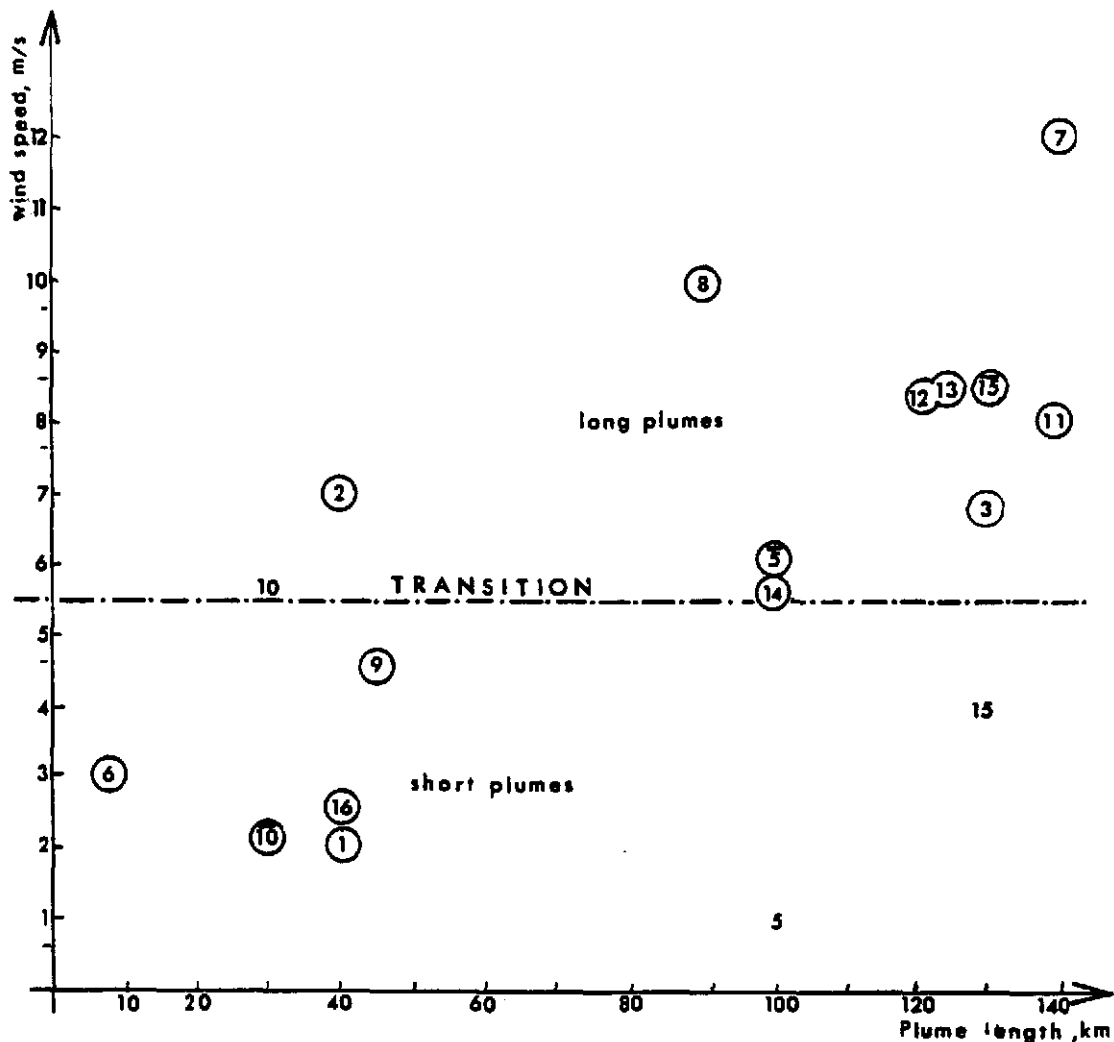
Figure 3.8. Plume length versus wind speed. The numbers correspond to the plume case (see table 3.2.). A dash over the case number indicates altitude data correction (uncorrected values without circles).

have more than 40 Km. A larger number of long plume images would be necessary before any conclusion about these two variables is reached.

In other words, for daytime conditions, local effects such as convection or ground turbulence seem to influence the spreading of the plume only with winds up to 5 m/s. Above this value the streamlines of synoptic flow prevail.

The preceeding conclusion seems to contradict the widely accepted dispersion equation for air pollutants in the atmosphere. This equation, for points along the plume's center line, is normally presented as:

$$X(x,H) = (Q/\pi.\sigma y.\sigma z.u)exp[-\tfrac{1}{2}(H/\sigma z)^2] \qquad (9)$$

where:

$X(x,H)$ is the pollution concentration in the plume, $[ML^{-3}]$, at downwind distance x, $[L]$, and for as effective plume height H, $[L]$.

σy and σz are the horizontal and vertical dispersion coefficients, $[L]$, both a function of downwind distance and atmospheric stability class.

u, the wind speed, $[LT^{-1}]$.

Q, the source emission rate of pollutants, $[MT^{-1}]$.

This equation can actually be separated in two parts: 1) $Q/\pi.\sigma y.\sigma z.u$, which is the continuity equation for the flow of pollutants and wind through a cross section defined by $2\pi.\sigma y.\sigma z$, and 2) the exponential term, which establishes a

Gaussian distribution of pollutants around the center line.
The wind speed (in the first part) is inversely proportional
to the concentration, which contradicts the results of the
analysis presented above. The reasons for this apparent
contradiction is found in the rate of pollution emissions.
When the source is very strong, as in the case of these long
plumes, the amount of pollution and gases emitted is enough
to overcome any initial spreading along the wind direction.
It is as if the emissions are released in the atmosphere,
and as a "puff", start flowing together with the wind. This
effect must be limited by a critical wind speed above which
begins the dillution of the plume along the wind direction.
The highest wind speed found in this study was 12.0 m/s (140
Km long plume) and it is below this speed limit.

The next step is to determine how this information can be
used in the field of air pollution modeling and forecasting.
The lateral dispersion of long plumes seems to be bounded by
a small angle with its origin at the source. In Figure 3.1,
for example, this angle is about 5°. In most cases, the
center line of this angle is not a straight line, and it may
be slightly curved (Figure 3.6) or segmented (Figure 3.4).
The departures from a straight line are related to synoptic
wind patterns. In all of the patterns, however, the lateral
spreading does not semm to vary too much.

The spreading angle which contains the long plumes
detected by the MSS varied from about 5° to 7.5°. The

expected concentrations are then obtained through the law of mass conservation. If the mass of the pollutants is conserved, assuming uniform dispersion along both downwind and crosswind axes,

$$Cp = Q/(u \cdot A), \tag{10}$$

where:

Cp is the concentration in the plume, $[ML^{-3}]$.

Q is the pollution emission rate, $[MT^{-1}]$.

A is the cross sectional area of the plume at a downwind distance x, $[L^2]$.

u is the mean wind speed at chimney height, $[LT^{-1}]$.

(A similar "simplistic" view of dispersion can be found in Scorer, 1978.)

For different and regular plume shapes, assuming constant wind speed along the plume's trajectory,

$$Cp = 4 \cdot Q/(\pi \cdot u \cdot \alpha^2 \cdot x^2), \text{ (circular cross s.)} \tag{11}$$

$$Cp = 4 \cdot Q/(\pi \cdot u \cdot \alpha \cdot \beta . x^2), \text{ (elliptical cross s.)} \tag{12}$$

where

x is the downwind distance, $[L]$.

α is the horizontal spreading angle, radians.

β is the vertical spreading angle, radians.

Since α and β are small, it was assumed that $\alpha=\tan\alpha=2\tan(\alpha/2)$. And introducing the limits of α (0.087 to 0.131), equation (11) corresponds to:

$$74.3 \cdot Q/u \cdot x^2 < Cp < 167.2 \cdot Q/u \cdot x^2 \qquad\qquad (13)$$

Another equation can be developed if the effect of the wind speed on the initial dilution of the plume is neglected. This condition is the same as assuming that the plume is discharged at the plume effective height by a horizontal chimney aligned with the wind, and with a speed equal to that of the wind. In other words, the initial pollution concentration is assumed to be so high that the initial dilution due to the wind is very little. If so, for a plume with circular cross section,

$$Cp = Cs \cdot Ds^2/Dp^2 \qquad\qquad (14)$$

where

Ds is the stack diameter, [L].

Dp is the plume diameter at a selected downwind distance, [L].

Both equations (13) and (14) assume uniform pollution distribution in the plume's cross sections. Refinements of this approach, like a Gaussian distribution or pollution decay or removal, can be obtained through common exponential terms.

The conclusion that the longer plumes occur with winds above 5 m/s can also be used to air pollution forecasting. From a complete wind rose, it is possible to find the frequency of time that the wind from any specific direction is above 5 m/s. This frequency can be used as an indication

Table 3.2. Dimensions of plumes in 17 Landsat images and meteorological parameters. See also next page.

A	B	C	D	E	F	G	H	I	J	K	L	M	N	O	P	Q	R
Case No.	Date & Time (GMT)	Plume length (Km)	Mixing height (Km)	Wind direc. at 10m	Wind speed at 10m (m/s)	Wind direc. up.air	Wind speed up.air (m/s)	Rel. humid at 10m (%)	Rel. humid. up.air (%)	Wind veri. 24hs (deg)	Δt/Δz (°C/Km)	Δθ/Δz (°K/Km)	Pasquill class	σy20(Km) Actual Pasq. Ratio	σy40(Km) Actual Pasq. Ratio	σy80(Km) Actual Pasq. Ratio	σy120(Km) Actual Pasq. Ratio
1	Aug/14/73 (12:16)	40	?	SW	2.0	?	?	88	?	90	?	?	A/B	0.5 / 2.5 / 4.9	0.7 / 6.0 / 2.8	1.9 / 5.1 / 2.7	2.3 / 8.0 / 3.5
2	Feb/10/73 (12:15)	40	?	SW	7.0	?	?	86	?	180	?	?	C/D	0.7 / 3.9 / 3.9	2.6 / 2.8 / 1.7	0.7 / 9.0 / 12.9	
3	Jun/23/74 (12:12)	130	?	NE	7.0	?	?	78	?	0	?	?	C	3.9 / 0.5 / 1.6			
4	Mar/13/75 (11:59)	ud	1.6	C	0.0	NNE (.7)	4.0	81		45	-6.9	3.6	A/B	0.7 / 2.3 / 3.3	0.7 / 5.1 / 7.1	0.7 / 9.0 / 12.9	2.1 / 8.8 / 3.8
5	Apr/18/75 (11:57)	100	1.7	N	1.0	N (.5)		61	60	180			A		0.7 / 4.0	1.4 / 5.1 / 3.6	
6	May/24/75 (11:55)	8	2.9	E	3.0	NE (.8)		?					B	0.5 / 3.2	0.7 / 8.0		
7	Aug/22/75 (11:50)	140	0.5 (7.3)	N	12.0	N (.5)	12.0	75	43	90	3.7 (-4.9)	13.0 (5.5)	C	1.3 / 1.8 / 6.9	3.5 / 3.9 / 1.2	2.1 / 5.5 / 2.4	2.8 / 8.0 / 2.9
8	Sep/09/75 (11:49)	90	0.5 (4.2)	N	10.0	NE (.8)	10.0	79	32	90	7.0 (-4.6)	2.2 (5.5)	C	0.9 / 1.4 / 1.6	1.4 / 2.8 / 2.0	2.0 / 5.1 / 2.5	2.9 / 1.8 / 1.9
9	Dec/08/75 (11:44)	45	- (4.1)	NE	4.6	N (1.1)	5.8	78	66	0	-5.3	4.7	B/C	1.0 / 1.8 / 1.7	1.1 / 5.3 / 4.2		1.8 / 4.2
10	Feb/18/76 (11:39)	30	- (4.2)	N	5.8	NW (1.0)	8.0	74	54	0	-4.8	5.3	C/D	1.0 / 1.8 / 1.0	2.2 / 2.8		
11	Mar/07/76 (11:38)	140	- (7.2)	NE	8.0	NW (.5)	8.3	76	34	0	-5.7	7.2	C	1.9 / 1.5	1.0 / 2.5		
12	Jun/23/76 (11:30)	120	0.5 (4.1)	N	8.3	NW (1.5)	8.3	81	25	0	5.7 (-2.4)	2.6 (7.8)	C	6.0 / 1.5	2.6 / 6.0		
13	Sep/03/76 (11:24)	120	4.7	NE	8.3			72		90	-6.1	3.9	C	0.5 / 2.1	2.4	4.6	4.2
14	Feb/21/77 (11:50)	ud	-	NE	5.8	N (.5)		73		0			C/D				
15	Mar/11/77 (11:49)	130	- (5.2)	NE	4.1	N (.5)	4.1	71	40	0	-5.8	4.2	B	1.4 / 1.6	1.4 / 2.9	4.0 / 5.0	1.9 / 10.0
16	Jun/09/77 (11:44)	40	- (4.1)	W	2.5	W (4.1)	2.5	80	10	90	-4.8	5.4	A/B	0.7 / 2.5	0.7 / 4.6		5.6
17	Jul/15/77 (11:42)	ud	0.5	NE	3.3			?					B/C				

Table 3.2, continued.

Observations:

- "ud" on Column C means that the plume length is undefined, either because the plume made a 180 degrees turn (case 4) or because its length could not be properly measured (cases 14 and 17).

- "?" on Column D and other columns corresponds to non-existent data.

- "-" on Column D means that there were no temperature inversions in the sounding data.

- The numbers in parenthesis on Column D were used as an upper limit to calculate temperature gradients of Columns L and M.

- On Column G, the numbers in parenthesis indicate the altitude in Km at which the corresponding wind direction was about the same of the plume. These altitudes also refer to the data on Columns H, I and J.

- Column K shows the variation of wind direction during a period of 24 hs before the Landsat images were obtained.

- On Columns L and M, the numbers in parenthesis correspond to the temperature gradients found when the mixing height in the parenthesis of Column D are used. Column M shows the potential temperature gradient.

- The Pasquill classes on Column N correspond to the standard Pasquill stability classes (Turner, 1968, for example).

- Columns O - R show the values of σ_y in kilometers for downwind distances of 20, 40, 80 and 120 Km. Actual values were measured from the images, the Pasquill values are from the Pasquill-Gifford graphs (Turner, 1968), and the Ratio values correspond to the Pasquill values divided by the Actual values. For the measured values it was assumed that the width of the plume is equal to $4.3 \cdot \sigma_y$ (Turner, 1968). This assumption considers the limits of the plume with 10% of the centerline concentration.

of the percentage that "ribbon-type" long plumes will occur. This percentage, in West Lafayette, IN, for example, is 25% for all directions combined (ground level).

Comparison With Other Data

The comparison of this work with others found in the related literature is limited by the shortage of experimental data for long plumes of industrial origin. The following three points are comparable:

1)The long plume discussed in the previous pages is not an isolated case. Randerson (1977), in a Skylab photo of the Louisiana coast, discussed a plume at least 140 km which resembled the long plumes found in Southern Brazil. Such long plumes were also reported over land and water surfaces (Millan and Chung, 1977).

2)Long plumes seem to occur with winds stronger than 5 m/s. For the 140 km plume of Randerson (1977), the mean flow was 8 m/s. For a presumed 400 km plume over Canada (Millan and Chung, 1977), the wind speed was above 6 m/s. For a 120 km plume along Long Island Sound, N.Y. (Brown et al., 1972), the wind speed was about 9 m/s. And for the case of two plumes with more than 300 km reported by Gillani et al. (1978), one had the wind always above 6 m/s; for the other, the wind varied from 4.0 m/s to 12 m/s.

3)The spreading angle for long plumes, from about 5° to 7.5°, seems to be valid from photographs of plumes. The previously mentioned cases of Randerson (1977) and Millan and Chung (1977) are within these limits. The same is also valid for many other cases, like those of Hilst, (1957), Randerson et al. (1971) and Torsani (1981) —all these only for the initial part of plumes. Nonhebel (1960) reported the vertical spreading angle very close to chimneys to be about 10°. He did not refer to the horizontal spreading angle. Brown et al. (1972) found this angle to be 23° for a 120 km plume. Since their evaluation was based on actual sampling, this cannot be compared with photographic techniques. It may, however, provide an indication of the difference between these two techniques. Scorer (1959) studied the initial spreading of plumes and arrived at the experimental value of 24°. He stated that this angle "has to be determined by experiment because the motion is too complicated for any existing analysis to determine it theoretically".

The small angle herein presented implies that long plumes disperse relatively little, and that pollutants may remain concentrated in the atmosphere for periods of several hours when the wind speed is high. An impressive example of this claim is found in the experiments of Moore et al. (1954). The comparison between this thesis and their work is almost impossible since they used balloons (and not plumes) at

about 9,100 m of altitude and with winds of more than

20 m/s. Nevertheless, it is worth remembering their

results. In the extreme case, two balloons released

together at ground level were only one mile apart after

traveling 1,930 km across the U.S.A. for 20.2 hours. For

the longest trajectory, 2.640 km, a pair of balloons was 29

miles apart. The horizontal spreading angle for these

experiments with pairs of balloons varied from about 0.54°

to 0.05°.

A comparison of the horizontal dispersion coefficients

measured from the Landsat images with those tabulated by

Pasquill-Hay-Gifford, or, "PHG" (Turner, 1968, for example)

is included in Table 3.2. The measured coefficients are up

to one order of magnitude smaller than the PHG values, and

this can be interpreted in three possible ways. First, such

variation is within deviations expected in experimental

work, particularly in the case of a long plume (see Islitzer

and Slade, 1968). Another possibility is that because of

the small concentration of pollutants at the edge of the

plume at long downwind distances, the Landsat sensors could

not detect the real outline of the plume. Although this can

occur to a certain extent, it cannot account for the whole

variation. At closer distances of the source (20 Km) the

plume outline is better defined than for longer distances

(120 Km) but the spreading angle seems to remain about the

same for all downwind distances. Therefore, it does not

seem possible that the real width of a long plume is up to ten times larger than the measured values. And a last possibility is that the PHG overestimate the dispersion coefficients. This last view seems most reasonable since the PHG are extrapolated from land experiments in the 1 Km range (Pasquill, 1961).

Gifford's equations in Chapter 2 (11 to 15) were also developed within the spirit of "no assumptions" regarding the plume. They provide a link between the widely used σy's and the shape of the plumes in these large-scale photos. The main limitation of Gifford's equations is the lack of necessary precision to measure Ym. This limitation can be reduced by working with digital enlargements of sections of the plume (see Figures 4.7 and 4.8 in the following chapter). The use of Gifford's equations resulted in σy's that showed no apparent relation with the commonly accepted Pasquill-Gifford (P-G) classes (Setzer, 1981). This could be because the P-G classes were obtained from limited data in the 1 km range.

Conclusion

The conclusions from this chapter can be summarized as follows:

-Landsat, as well as other satellite imagery, provides synoptic views of some air pollution plumes when no cloud cover exists, and which are very difficult to obtain from

terrestrial instruments. The dimensions of plume cross section and relative density can be obtained from these images but with certain limitations. Plume length and shape seem to be the parameters obtained with fewer restraints.

-The dispersion of plumes over an open ocean seems to be mainly a function of the wind speed.

-No apparent relation was found between the plume length, chosen as a dispersion indicator, and the A-F stability cases of the P-G system of dispersion.

-σy's values for the same plume varied based on the equation . used in their evaluation. This fact was interpreted as an indication that current methods of dispersion calculation do not provide a good explanation of the physical phenomena behind medium-range transport of pollutants.

-A new approach to the medium range transport of air pollution plumes (up to 200 Km) is suggested. The plumes are seen as an indication of the flow regime, as in Reynolds' early experiments with fluid dynamics. A spreading angle of 5° to 7.5° seems to contain the parts of the plumes which are detected in small scale photographs.

-This range for the horizontal spreading angle, and the wind speed limit of 5 m/s appears to be in agreement with other data for long plumes found in the literature.

The length and shape model of long plumes presented above may have broad applications. When and if this model is accepted, based on the study of a large additional number of plume images, it may be used for estimates of long plume dispersion. This is a subject of great interest (acid rain, e.g.), and in which very few experiments have been made. Another point, shown in the next chapter, is that some plumes over water bodies and recorded in multi-spectral images can be analyzed by a computer, without human interpretation of the images. And combining these possibilities, it will be feasible to develop an automated system that will continuously monitor long plumes and also make dispersion estimates.

CHAPTER 4

A LARSYS INVESTIGATION OF A LONG PLUME

Introduction

This chapter shows the results of the use of the LARSYS software for a Landsat image of an air pollution plume over Lake Michigan. LARSYS, a software package for remotely sensed multispectral data, was developed at the Laboratory for Applications of Remote Sensing (LARS), Purdue University. This technology was conceived in the mid-1960's and well established in the early 1970's with the launching of the Landsat-1 multispectral scanner (MSS).

The objective of this chapter is to show that air pollution plumes spreading over water can be identified by "unsupervised" classification techniques. An unsupervised classification does not require previous knowledge of the location of the object(s) of the investigation nor of its optical spectral characteristics. The basic requirements for using this technique are: 1) that the object of interest must have its spectral signature statistically different from other surrounding ground covers, and 2) that the classification results can be associated with "ground

truth." Concerning the latter, the characteristic shape of pollution plumes provides a good way to corroborate their presence. As for the first condition, the following pages show that plumes over water have their own spectral characteristics.

All the programs used in the digital analysis that follows are described in LARS (1973, and 1980).The pictures of the plumes were obtained by photographing digital images from the screen of the COMTAL ONE-20 VISION (COMTAL, 1980) at LARS.

The Gary Plumes

Figures 4.1 and 4.2 show air pollution plumes originating close to Gary, IN, and spreading over Lake Michigan. These figures are portions of Landsat frames (see their legend and captions). Figures 4.3 to 4.6 show the same scene as Figure 4.2 but separated according to the four Landsat MSS bands. Figures 4.7 and 4.8 show successive digital enlargements of Figure 4.2 where individual picture elements ("pixels") are noted. Only the plumes of Figure 4.2 will be used in this chapter since the results from the analysis of Figure 4.1 were basically the same as those of Figure 4.2. See Appendix A for average emission data of the air pollution sources associated with these plumes.

Table 4.1 shows the average values and standard deviations for land, plume, and lake pixels of the lower-

left corner part of Figure 4.2. These values were obtained from the 3-classes Cluster analysis - see Figure 4.14. The table also shows the range of reflectance values, the difference in reflectance values for water and plume pixels, and the ratio of these two values. Band 5 has the highest value for the difference of the average of plume and lake pixels, which indicates a better contrast for the plumes in this band as compared to other bands. When the range of reflectance values (maximum values) for each band is also considered, as in the case of the maximum reflectance value to the difference of plume and lake pixels, band 5 still shows the highest value. A corroboration of this result is found in Figures 4.3 to 4.6, where one can see that the band 5 image (Figure 4.4) shows a better definition of the plumes.

Table 4.1. Comparison of land, plume and lake pixels on a Landsat image of a long air pollution plume.

	Band 4 (0.5-0.6u)		Band 5 (0.6-0.7u)		Band 6 (0.7-0.8u)		Band 7 (0.8-1.1u)	
max.reflectance	0-37/128		0-39/128		0-43/128		0-23/64	
plume-lake difference	2.56		3.37		2.58		1.40	
max.val./diff.	0.069		0.086		0.060		0.061	
mean; variance	$\bar{X}$	s	$\bar{X}$	s	$\bar{X}$	s	$\bar{X}$	s
Land	26.50	8.96	22.10	13.01	18.74	18.20	6.77	5.65
Plume	23.50	4.07	13.62	3.65	8.90	5.05	2.21	1.46
Lake	20.94	1.10	10.25	0.47	5.32	0.93	0.81	0.33

For the "maximum reflectance" values, the number after the slash is the total possible range of the band.
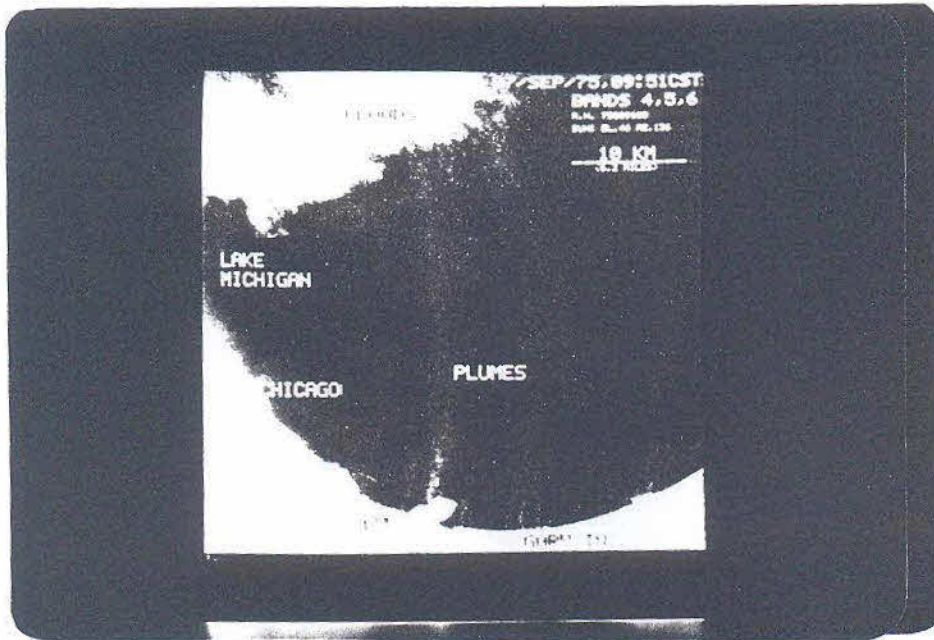
Figure 4.1. Landsat image showing the Gary air pollution plumes over Lake Michigan; bands 4,5, and 6 combined. See Appendix A for the corresponding meteorological data.
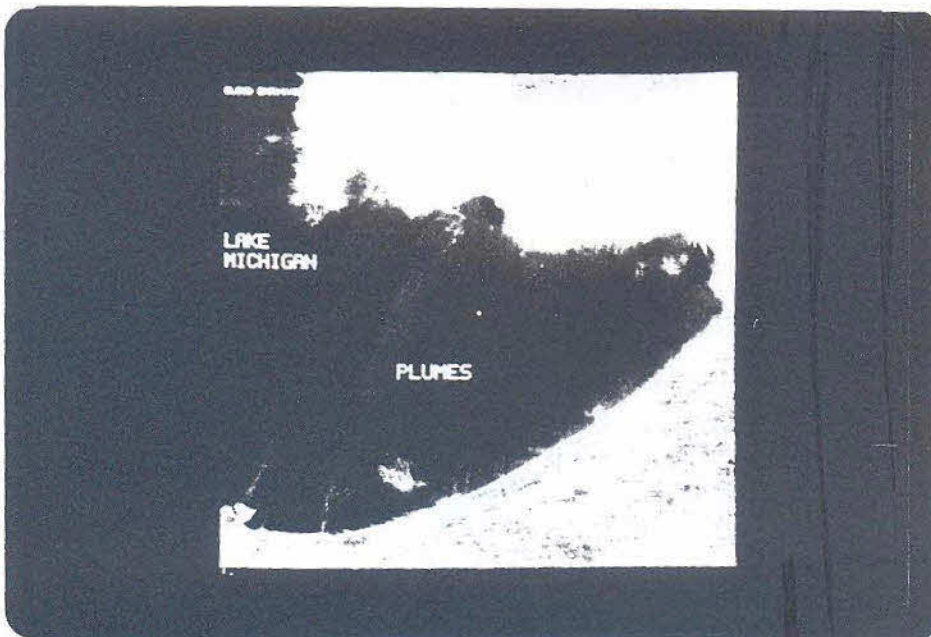
Figure 4.2. Another case of the Gary plumes. Landsat image of Oct./01/72; bands 4,5,6 combined. See Appendix A for the meteorological data.

Figure 4.3. Band 4 (0.5-0.6u) image of the plumes of Figure 4.2.

Figure 4.4. Band 5 (0.6-0.7u) image of the plumes of Figure 4.2.
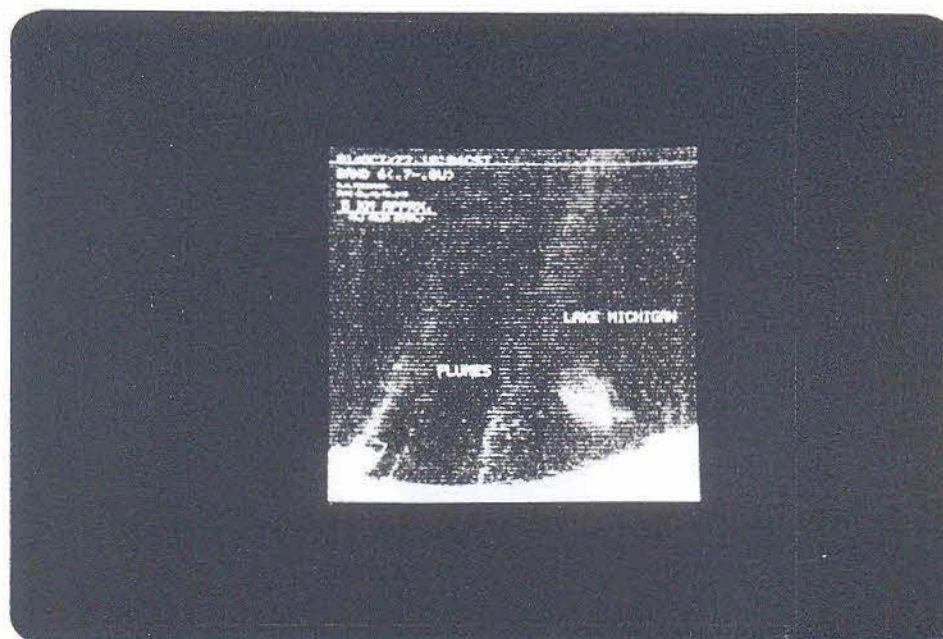
Figure 4.5. Band 6 (0.7-0.8u) image of the plumes of Figure 4.2.
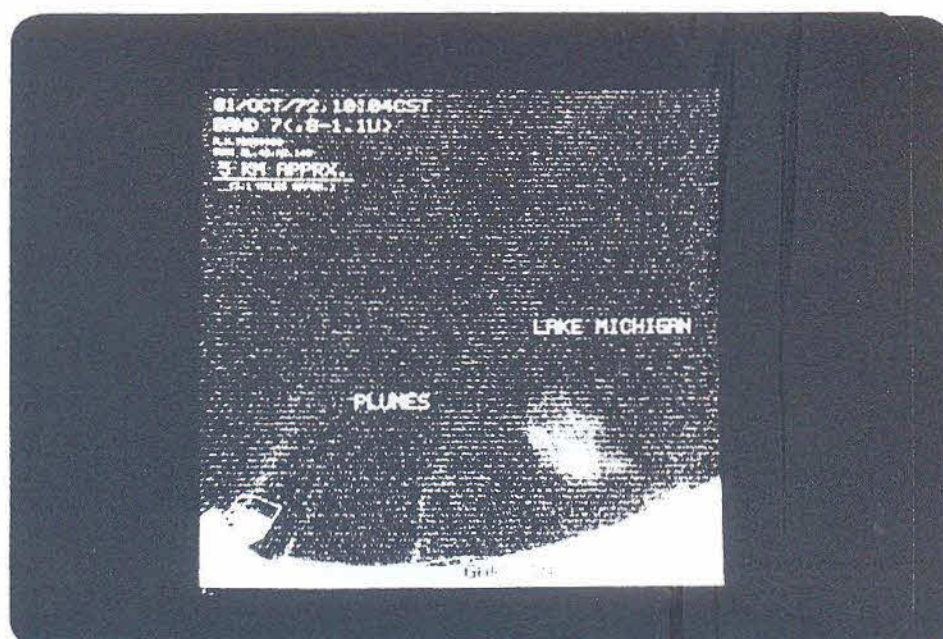
Figure 4.6. Band 7 (0.8-1.1u) image of the plumes of Figure 4.2.
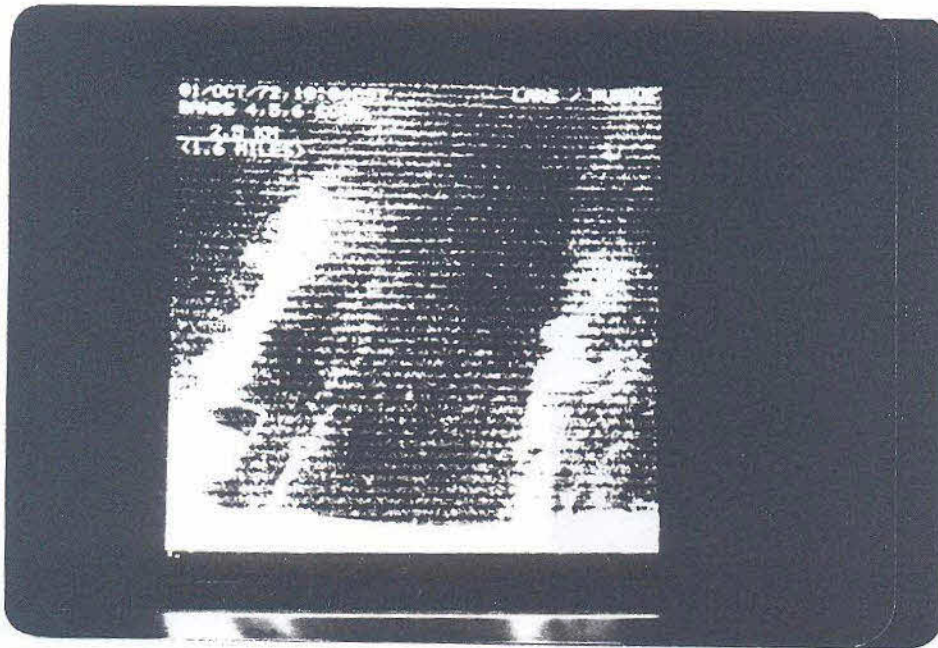
Figure 4.7. Digital enlargement of Figure 4.2.
Bands 4,5,and 6 combined.
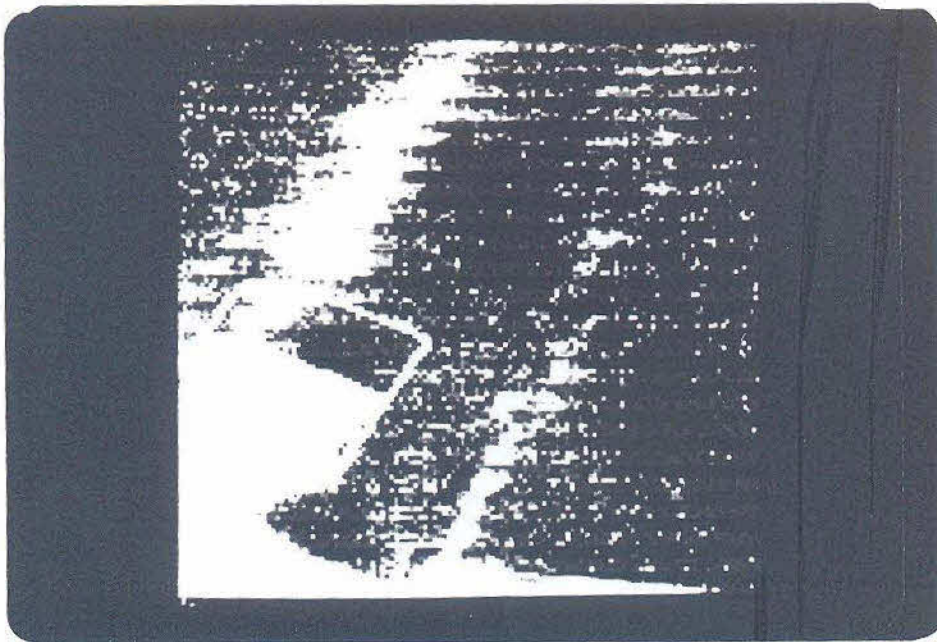
Figure 4.8. Digital enlargement of Figure 4.2 and
4.7. Note that individual pixels are visible; bands
4,5, and 6 combined.

Pictureprint

The LARSYS "Pictureprint" function reads data from multispectral image storage tape and produces alphanumeric pictorial printouts of the data for each channel specified (LARS, 1973).

Figures 4.9 and 4.10 show such printouts for channels 2 and 3, respectively, and they correspond to portions of Figures 4.4 and 4.5. Note that for channel 3 (Figure 4.10) the lines 1306, 1312, 1318 and so forth show a regular pattern. This is noticeable in the right margin of the figure but disappears over the plume. This "striping" is due to problems with calibration in the early Landsat data, but does not seem to be strong enough to affect the recording of the plumes. Another feature of Pictureprint is that many plume and land pixels are depicted by the same symbol. This effect can be reduced if the range of reflectance represented by each symbol is "stretched", which requires a time consuming work.

Figure 4.9. "Pictureprint" result for band 5.

Figure 4.10. "Pictureprint"result for band 6.

Linegraph

The LARSYS "Linegraph" function graphs data values from requested lines of a multispectral image storage tape (LARS, 1973). Figure 4.11 shows the output of Linegraph for a crossection of the left plume in Figure 4.2 We can see that the energy levels of the pixels of the plumes are just slightly higher than those of the water. Pixels of band 4, represented by "1", had the high energy values for both water and plume, while band 7 had the smallest.

An explanation of these facts is that water reflects very little energy in the near-infrared band 7, and that plumes tend to be transparent in this region of the spectrum. The little variation in the pixel energy levels caused by the plume in the other 3 bands shows that the plume is barely detectable by the Landsat MSS. Of the 128 existing levels of energy (64 for band 7), the plume caused a maximum variation of about 3.

Figure 4.12 contains Linegraph results for a line immediately adjacent to one represented on Figure 4.11, and also shows that variations in the pixels do occur from line to line. The variations, however, are small (about one level of energy) and one cannot be sure about their meaning because they are very close to the sensitivity limit of the MSS.
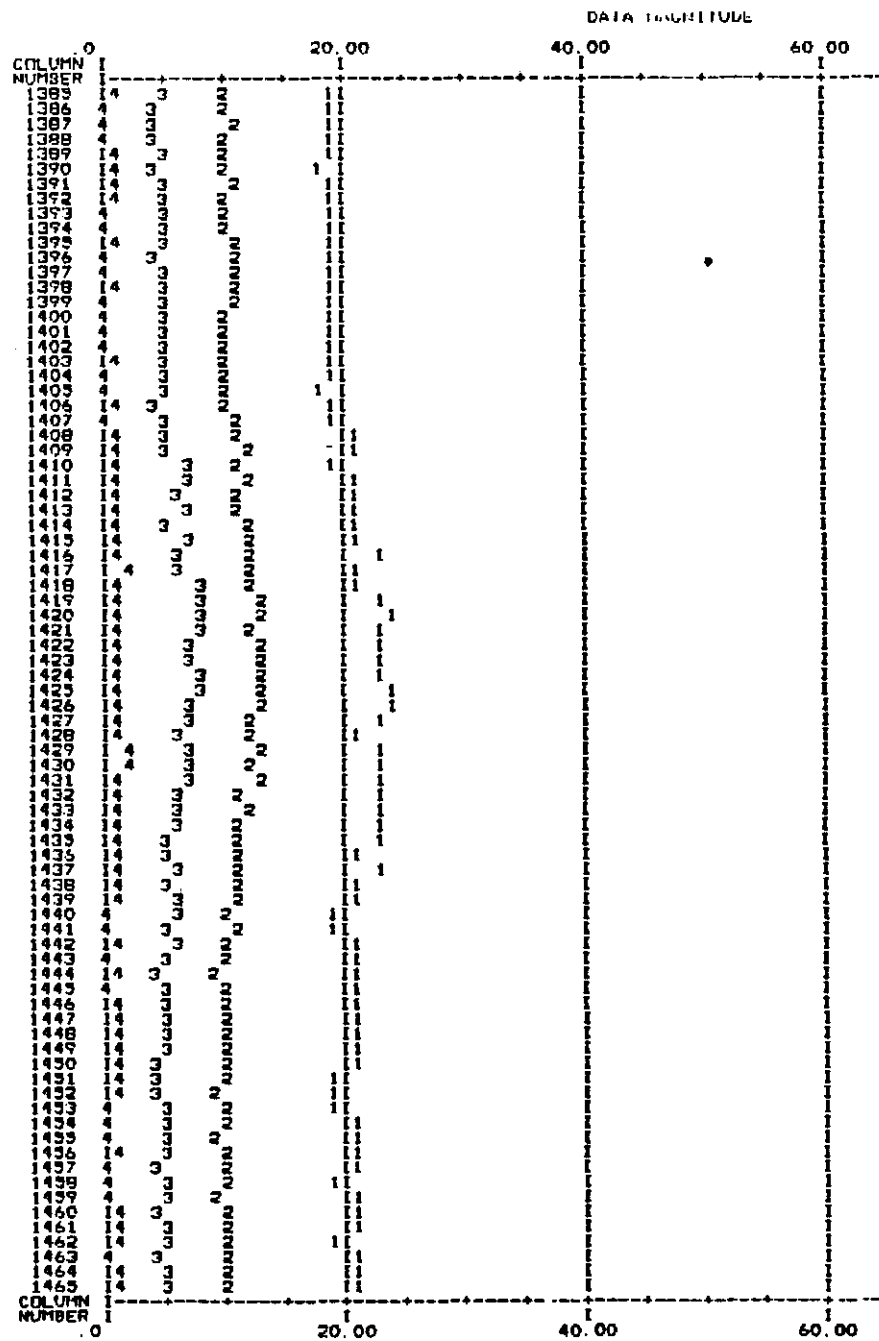
Figure 4.11. "Linegraph" result for line 1326.
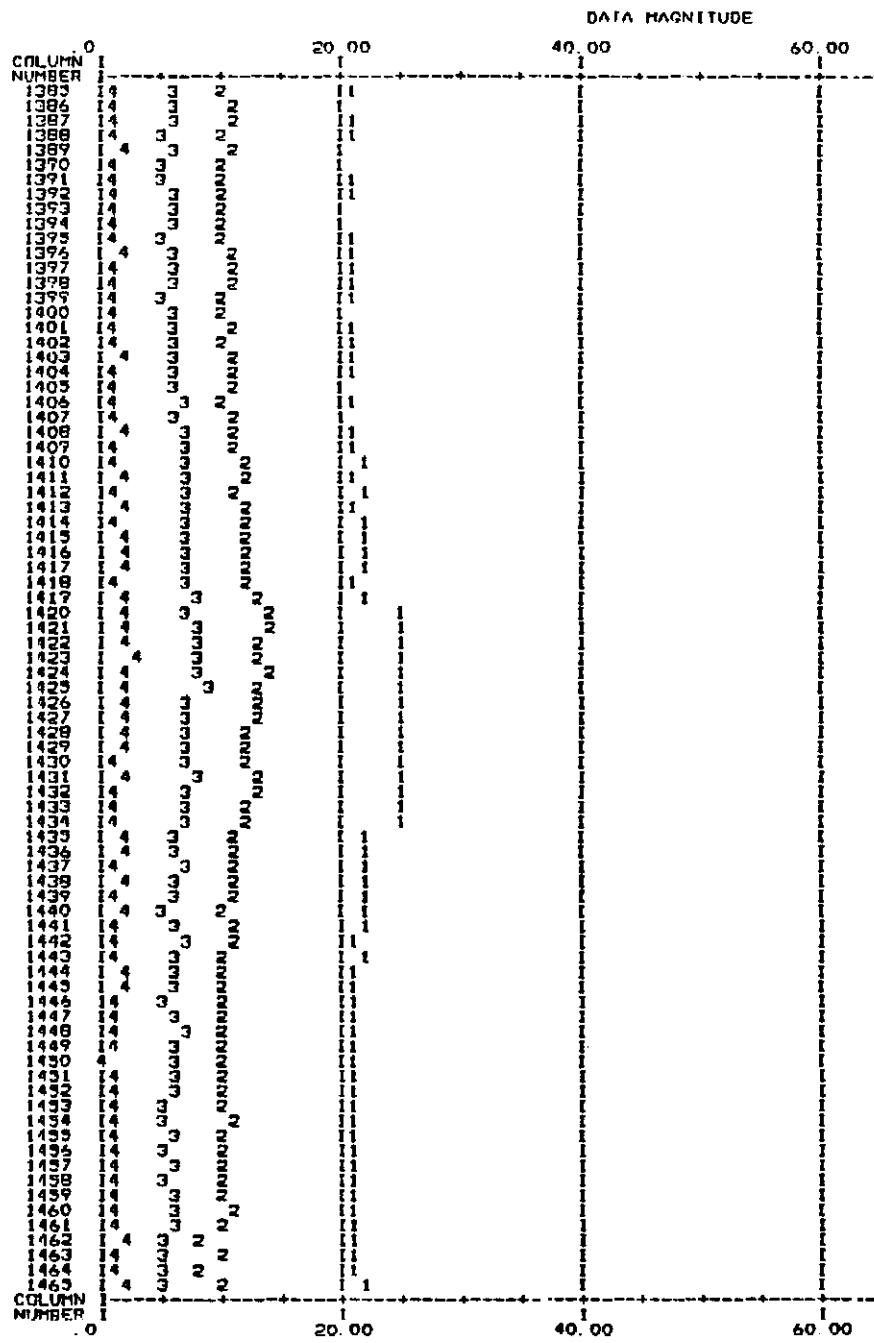
Figure 4.12. "Linegraph" result for line 1327.

Cluster

The LARSYS Cluster function implements an unsupervised classification (Clustering) algorithm which classifies individual data points into number of classes (clusters) defined by the analyst. The algorithm is based upon the distance relationships between each point and the centers of groups of points (Clusters) in an n-dimensional space defined by the n spectral bands used (LARS, 1973). All the following Clusters were prepared using the 4 Landsat bands. A convergence of 98.5% was chosen in order to keep a relatively low computer processing time. This parameter is defined in terms of the percentage of samples whose classification is unchanged from the last iteration (LARS, 1973).

Figure 4.13 shows the results of a Cluster in which only two distinct classes were specified. One class, is represented by blank spaces, corresponds to land. The second class, the water, is shown as "m". The plumes are not seen in this example because the Clustering could not classify them as one of the two more distinct classes.

Figure 4.14 shows the result of a Cluster where 3 classes were specified, and where the plumes were represented as an independent class. This was interpreted as a proof that, although the reflectance of the plume is close to that of water (see Linegraph above), it is different enough from

that of water to be separated by an unsupervised classification algorithm.

Figures 4.15, 4.16, 4.17 and 4.18 show Clusters where 4, 5, 6 and 15 different classes were specified, respectively. We notice that the plume becomes wider with a higher number of classes. This means that with more classes that the Clustering algorithm was able to define parts of the plume with different reflectance characteristics, in a probable association with variations in pollution concentrations. The results of another Cluster for which 15 classes were specified are shown in Figure 4.19. In this case, the area of study included a good portion of the shore of Lake Michigan. The results, however, showed that the maximum number of different ground cover classes that could be statistically separated was 8, not 15. Figure 4.19 shows these 8 classes, of which one is related to the plume. Therefore, we can see that plumes over water are found in unsupervised classifications even when a more diversified ground cover exists. In Figure 4.20, the result of a 15-class cluster is shown for a region of the image which did not include land. In this case the algorithm was again able to clearly separate the plume from the lake background.

For a 6-classes Cluster the pixels classified as plume are also found scattered all over the area examined. This is interpreted as an indication that for six classes the Clustering result is subject to noise in the data.

Therefore, for technical as well as for low cost considerations it is suggested that Cluster studies of plumes be made with five classes (63.3 seconds of CPU time).

Figure 4.21 shows a bi-spectral graph for the fifteen classes of Figure 4.17, and obtained with the "mergestatistics" (LARS, 1980) processor. The classes A-E of Figure 4.21 (or 1-5 in Figure 4.18) correspond to ground covers over land; classes F-I (6-9) to the plume, and classes J-O (10-15) to water. The actual statistical differences between any of these classes are obtained from the "Separability" processor below.

89

Figure 4.13. "Cluster" result for only two classes (lake water and the harbour)

Figure 4.14. "Cluster" result for three classes. The air
pollution plumes are represented by the "*".

Figure 4.15. "Cluster" result for four classes. Note that noise in the Landsat data is noticed mainly through the "M" symbols.

Figure 4. 16. "Cluster" result for five classes. Note that the water break and the plumes are classified with different symbols.
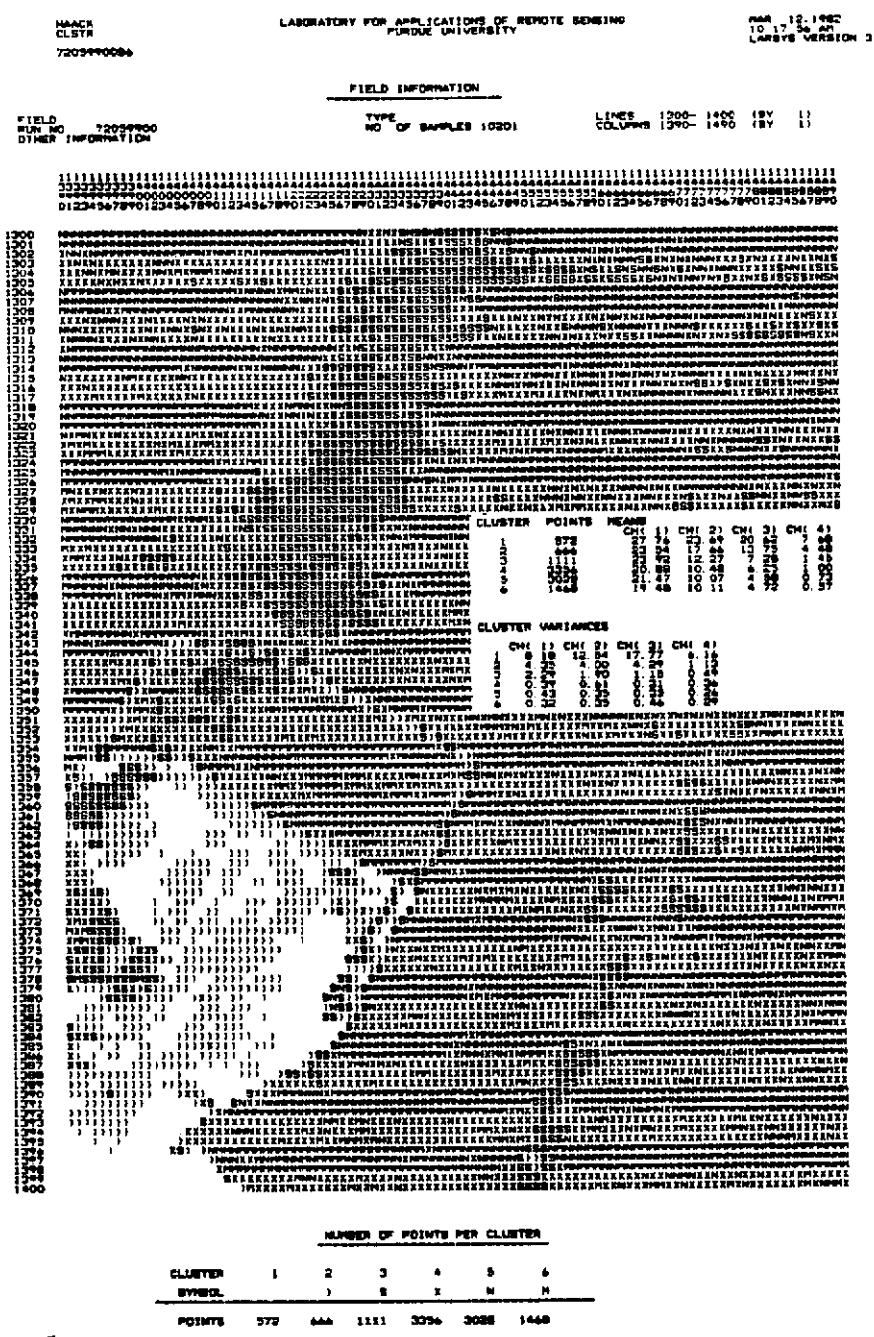
Figure 4.17. "Cluster" result for six classes. Although the plumes seem wider, the symbols "x" are found everywhere. Note also that the "s" symbols, which represent the plume, are less numerous than the "*" symbols in Figure 4.16.

Figure 4.18. "Cluster" result for fifteen classes. Note that although the plumes are represented mainly by three classes, "I", "T", and "Z", the "Z" class is also common to other regions.

Figure 4.19. "Cluster" result with eight classes obtained from fifteen original classes. This reduction, set by the Clustering algorithm, was due to the increase of land area.

Figure 4.20. "Cluster" result for fifteen classes of plume and water only. The actual existence of these fifteen classes is questionable.

Figure 4.21. Bi-spectral plot (Bands 4 & 5 versus 6 &7) for the fifteen classes of Figure 4.17. Classes A-E correspond to land, F-I to the plumes, and J-O to water. This graph helps to visualize the reflectance characteristics of the spectral classes. Note how water and plume classes are very close, which may indicate that it is relatively difficult to draw a clear boundary between these two classes. This graph was produced by the "Mergestatistics" processor (LARS, 1980).

Separability

The LARSYS Separability function uses class statistics to calculate measurements of how well any two individual ground cover classes may be distinguished, or the degree of "separability" between the classes ("divergence"). The separability function also helps to select the set of channels that will produce the most accurate classification by the Classifypoints function (LARS, 1973).

As a rule of thumb, transformed divergence values close to 2,000, the limit value at which point they are indicative of very good class separability, while values around 1,500 reflect relatively poor class separability. Table 4.1 shows the separability divergence values for the classes of Figures 4.17 and 4.21 when the four Landsat bands are considered. This table shows that only classes "M" and "N" had their separability divergence below 1,500. A few cases had divergence values below 1,750, e.g., "B" and "C", "C" and "D", "F" and "H", "I" and "J", "K" and "L", "L" and "M", and "L" and "N". Divergences for the remaining two-class cases were above 1,750 and indicated that, from a statistical point of view, the classes could be separated.

Another tool to analyze the actual distinctions between the many classes obtained from a Cluster is the Biplot processor of LARSYSDV. The Biplot function is a capability that allows plotting in a two-dimensional feature space (of

MSS channels) the following: 1) the means, 2) the ellipses of concentration, and 3) the classifications of feature space for each class in a statistics file (LARS, 1980).

Figure 4.22 shows one example of these graphs for bands 4 and 5. The region in the lower part of the figure which corresponds to the air pollution plume was outlined. The examination of all such graphs for the 6 combinations of Landsat bands also contributed to the decisions about which classes can be deleted or pooled with other classes.

Table 4.2.Transformed divergence for the Separability function.

RETENTION LEVEL ..   1. MAXIMUM 30000   DIVERGENCE **WITH** SATURATING TRANSFORM
                        MINIMUM 0

	CHANNELS	DIJ(MIN)	D(AVE)	WEIGHTED INTERCLASS DIVERGENCE (DIJ)									
				AB (10)	AC (10)	AD (10)	AE (10)	AF (10)	AG (10)	AH (10)	AI (10)	AJ (10)	AM (10)
1.	1 2 3 4	1440.	1952	1834	1999	2000	2000	2000	2000	2000	2000	2000	2000

	CHANNELS	WEIGHTED INTERCLASS DIVERGENCE (DIJ)														
		AL (10)	AM (10)	AN (10)	AO (10)	BC (10)	BD (10)	BE (10)	BF (10)	BG (10)	BH (10)	BI (10)	BJ (10)	BK (10)	BL (10)	BM (10)
1.	1 2 3 4	2000	2000	2000	2000	1624	1857	1993	2000	2000	2000	2000	2000	2000	2000	2000

	CHANNELS	WEIGHTED INTERCLASS DIVERGENCE (DIJ)														
		BN (10)	BO (10)	CD (10)	CE (10)	CF (10)	CG (10)	CH (10)	CI (10)	CJ (10)	CK (10)	CL (10)	CM (10)	CN (10)	CO (10)	DE (10)
1.	1 2 3 4	2000	2000	1739	1779	1999	1977	2000	2000	2000	2000	2000	2000	2000	2000	1739

	CHANNELS	WEIGHTED INTERCLASS DIVERGENCE (DIJ)														
		DF (10)	DG (10)	DH (10)	DI (10)	DJ (10)	DK (10)	DL (10)	DM (10)	DN (10)	DO (10)	EF (10)	EG (10)	EH (10)	EI (10)	EJ (10)
1	1 2 3 4	1932	1972	2000	2000	2000	2000	2000	2000	2000	2000	1972	1771	2000	2000	2000

	CHANNELS	WEIGHTED INTERCLASS DIVERGENCE (DIJ)														
		EK (10)	EL (10)	EM (10)	EN (10)	EO (10)	FG (10)	FH (10)	FI (10)	FJ (10)	FK (10)	FL (10)	FM (10)	FN (10)	FO (10)	GH (10)
1.	1 2 3 4	2000	2000	2000	2000	2000	1809	1649	1999	2000	2000	2000	2000	2000	2000	1772

	CHANNELS	WEIGHTED INTERCLASS DIVERGENCE (DIJ)														
		GI (10)	GJ (10)	GK (10)	GL (10)	GM (10)	GN (10)	GO (10)	HI (10)	HJ (10)	HK (10)	HL (10)	HM (10)	HN (10)	HO (10)	IJ (10)
1.	1 2 3 4	1819	1994	2000	2000	1997	2000	2000	1908	1994	1974	2000	2000	2000	1986	1537

	CHANNELS	WEIGHTED INTERCLASS DIVERGENCE (DIJ)														
		IK (10)	IL (10)	IM (10)	IN (10)	IO (10)	JK (10)	JL (10)	JM (10)	JN (10)	JO (10)	KL (10)	KM (10)	KN (10)	KO (10)	LM (10)
1	1 2 3 4	1935	1989	1950	1779	1993	1899	1947	1842	1998	2000	1662	1921	1966	1966	1738

	CHANNELS	WEIGHTED INTERCLASS DIVERGENCE (DIJ)			
		LN (10)	LO (10)	MN (10)	MO (10)	NO (10)
1.	1 2 3 4	1677	1869	1460	2000	1999

Figure 4.22. "Biplot" result for bands 4 and 5. The outlined regions correspond to the air pollution plumes.

Classifypoints

After some ground cover classes were deleted or pooled, it was necessary to determine if the remaining classes could be used to identify the plume. This was done through the Classifypoints LARSYS processor which assigns the most probable class to each pixel and prepares the classification. The algorithm actually calculates the probability that the pixels belong to each of the ground cover classes defined (LARSYS, 1973).

In Figure 4.23 we have the results of Classifypoints using 8 classes. These classes were chosen from the Cluster with 15 classes (see Figure 4.18) representing the 3 ground covers of interest: land, plume and water. The Classification results, which assign every pixel to one of the eight chosen classes, did not provide as a good definition of the plume as has been found in the original 15-class Cluster. Before Classifypoints, the Mergestatistics, Separability, and Biplot functions were used for the 5 chosen classes in order to check their separability, which was good.

After many trials using 6 and 12 classes, and varying the classes while keeping the same total number of classes, and for each case using the Mergestatistics, Separability and Biplot functions, the following conclusion was reached: even when the divergence separability between classes is higher,

no classes should be disregarded or pooled; the spectral characteristics of the plume are so close to that of other ground covers that any alteration in the original classes found by the Clustering algorithm will have a negative effect on the Classifypoints function. This does not mean that less than 15 classes cannot be used for this plume with Classifypoints. The requirement for the use of fewer classes seem to be that the Cluster function be done with less than 15 classes (as in Figures 4.14 to 4.17). The total number of original classes in the Cluster will then have to be used with Classifypoints.
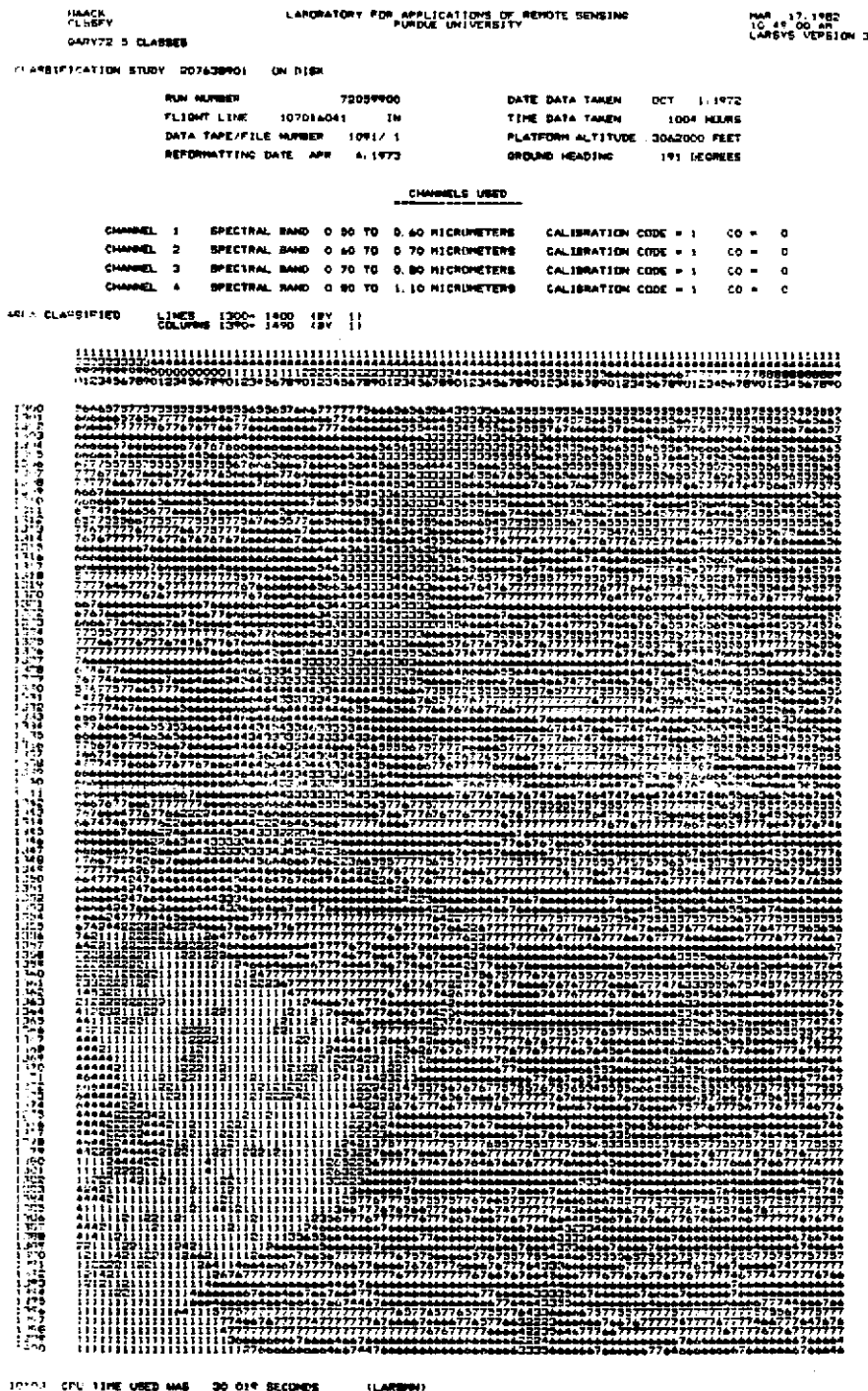
Figure 4.23. "Classifypoints" result for eight classes reduced from fifteen original classes. Note that the plumes are not visible.

Channeltransformation

Channeltransformation is a LARSYSDV program used to generate another spectral channel based on transformations of existing channels.

Figure 4.24 shows a computer printout of a new channel generated by dividing the values of the pixels in the Landsat band 5 by those of band 6 and then multiplying the results by a factor of 50. The physical meaning of any such transformation is questionable, although the results are known to provide useful information in many cases. In this case, we see that the air pollution plume is again visible over water. This result does not appear to make any significant contribution to what was already known from examining either the original channels or the unsupervised Clustering classification.

Figure 4.24. Result of the "Channeltransformation" function. Function = 50 x (band 5/band 6).

Conclusion of Chapter 4

In this chapter it was shown that air pollution plumes over water can be identified by an unsupervised Clustering classification. This fact, although already reported (Lyons 1974), had not been investigated in depth. The above study is an indication that plume research can be done in MSS data with a (relative) minimum of time and work expenditures. See also the conclusions presented on items 4, 5, and 6 in the next pages.

RESULTS AND CONCLUSIONS

This is a study about dispersion and imaging of long (10–200 Km) air pollution plumes, a field with limited experimental data. A thorough review of the literature, in itself a new and important contribution, revealed that current dispersion theories for plumes do not explain adequately the patterns of long plumes, and that analysis of computer-aided techniques to identify and map the extent of dispersion have not been developed. The following is a summary of the main results and conclusions found.

1. A regression fit between the length of a long air pollution plume spreading over the ocean in sixteen different cases and various meteorological parameters showed that wind speed is the prevailing meteorological parameter associated with the length of the plume.

    a. Plumes less than 50 Km in length occurred for wind speeds less than 5 m/s and showed an oscillating pattern which reflects the dominance of local convection at lower wind speeds.

    b. Plumes 150 Km in length were associated with higher

wind speeds and showed a ribbon-type flow pattern as contrasted with the oscillating nature of the short plumes.

c. These results contradict the widely used dispersion equations which assume that the dispersion of plumes in the atmosphere varies directly with the wind speed. On the other hand, this result agrees with the variation of the dispersion coefficients as a function of atmospheric stability (Pasquill classes), i.e., the higher the wind speed the smaller the lateral plume spread.

These results are explained based on two effects:

a. Winds above 5 m/s are able to dominate local convective effects which normally improve dispersion conditions.

b. The direct effect of wind speed on the dispersion, which is a premise of the basic continuity equation, does not take into account the size of the plume emitted in relation to the wind flow. In other words, with large scale sources like those studied, the significant amount of particulate pollutants emitted by the stack is of sufficient magnitude to minimize the initial dilution due to the wind flow (at least up to 12 m/s, the highest value found).

2.The values of the horizontal dispersion coefficients measured from the images are up to one order of magnitude smaller than the widely used corresponding Pasquill-Hay-

Gifford values. Such variation is normally expected in experimental work, and particularly for small scale images of long plumes. The Pasquill dispersion coefficients refer to all regions inside the plume where the pollution concentrations are higher than 10% of the concentration at the center line of the plume. With satellite images of long plumes, it is not possible, with the present technology, to determine the arbitrary 10% line, and the plume limits are considered to be along the visible borders of the plume. Long plumes are within a horizontal dispersion angle of 5° to 7.5°, which is used to estimate downwind concentrations based on the downwind distance, the emission concentration at the source and the height of the vertical dispersion layer. This angle is also observed in other images of long plumes found in the literature review.

3. Regression equations to fit the sixteen cases analyzed are developed for the determination of the visible lengths of the long plumes. The best-fit equation is:

$$X = 58.4 \ln V + 10.8 \qquad (1 < V < 15)$$

where X is the total length of the plume in Km and V the wind speed in m/s. These equations are subjected to modification with increase in sampling population.

4. The shape of a plume in the Landsat imagery analyzed in this study is more visible on the image of band 5 (0.6-0.7μ) than on the other bands. This is determined by comparing the ratios of the difference of the plume and

water average reflectance values to the maximum reflectance value. These ratios were 0.086 (3.37/39) for band 5, 0.069 (2.56/37)for band 4, 0.060 (2.58/43) for band 6, and 0.061 (1.40/23) for band 7. However, it should be noted that the best band to show plume outlines can vary among Landsat images because of variations in the plume and water background reflectance characteristics.

5. A computer-aided "Clustering" technique is effective in discriminating the long plumes analyzed in this study.

a. A Clustering algorithm that divides all spectral classes into three main ground covers is sufficient to discriminate a plume from water and land backgrounds. For a Cluster with six classes or more, pixels classified as plume also are found beyond the plume limits. This is interpreted as an indication that for six classes or more the Clustering result is subject to noise in the data. A Cluster with five classes is suggested as most applicable for this type of plume study. With more than five classes the plume is represented by more than one spectral class and is also wider, its boundaries are fuzzier because of the effect of the noise in the data.

b. For a 7.9 Km by 5.7 Km area with 10,000 pixels, the "LARSYS" Clustering program required the following CPU (seconds) on a IBM 4341 computer: 49.6 s for three classes, 63.3 s for five classes, and 143.4 s for fifteen classes. For the five classes Cluster, the corresponding

CPU cost was $10.80. This cost can also vary according to the computer used for the analysis.

6. A visual comparison between the multi-class Cluster technique and a simple digital printout of the original Landsat image ("Pictureprint") showed the Pictureprint (15.6 s. CPU) to produce results with poorer definition of the plume. The digital image depicts land and plume pixels as the same ground cover in many cases. Pictureprint results can be improved if the range of reflectances relative to the plume and water is expanded. However, this technique would require more human-computer interaction, thus increasing the cost of analysis.

FUTURE WORK

The results presented in Chapters 3 and 4 open many possibilities for future and original work, like:

-To analyze more satellite images of long plumes in order to verify the shape and plume length view developed in this work, and eventually obtain a final dispersion model for long plumes.

-To do measurements of concentrations of gases and particulates in a long plume at the same time that Landsat (or other satellite) is obtaining the multi-spectral image of the same plume. This will possibly allow the development of a relation between reflectance values of the plume and its pollution concentration.

-This study has shown that the widely used Gaussian equation of atmospheric diffusion seems not to fit the images of long plumes. The reasons for this discrepancy are thought to be in the values of the dispersion coefficients and in the equation itself (inverse effect of the wind speed). A deeper analysis of this work is necessary before a final conclusion is drawn. This could be done by examining in the equation, the variation of predicted concentrations as a function of wind speed in each stability

class.

-Since an unsupervised computer-aided technique can be adequate to discriminate a long air pollution plume, a next step would be to develop an algorithm to automatically decide wether a plume is present in a multi-spectral image. This algorithm could then be implemented into a continuous monitoring of environmental problems like forest fires, air pollution plumes, etc.

-Landsat multi-spectral scanner images exist for many parts of the world, covering a period of ten years. It is probable that an almost unlimited and unused amount of long plume dispersion data has been gathered and only need to be studied. Also, it was shown that the investigation of some long plumes can be done by a computer, without human interpretation, and with relatively low cost (50 to 134 sec. of CPU time on a 4341 IBM computer. Therefore, it is suggested that an automated program be implemented to locate long plumes and also make dispersion estimates.

LIST OF REFERENCES

LIST OF REFERENCES

Anson, A. 1968. Photographic interpretation from space. In Manual of color aerial photography, 1st ed., ed. by J.T.Smith, Jr. and A.Anson, 1968. Amer. Soc. of Photogrammetry, Falls Church, VA, pp.412-413.

Alcalis 1979. Personal communication.

Barnes, J.C., Bowley, C.J., Parr, J.T., and Smallwood, M.D. 1977. Snow mapping experiment. In Skylab explores the earth, by NASA L.B.Johnson Space Center; NASA publication SP-380. U.S.Governm. Print. Office, Washington, D.C., p. 216.

Barringer, A.R. and Davies, J.H. 1978. Remote sensing for air pollution control. Proceed. 12th internat. symp. on remote sensing of environment, v.I. Environm. Research Inst. of Michigan, Ann Arbor, MI, pp. 258-269.

Blais, R.N. 1974. Inherent limitations of monocular techniques for determining smoke plume parameters from aerial photography: an error analysis. In Remote sensing of earth resources, v.III, ed. by F.Shahrokhi. The Univ. of Tennessee, Tullahoma, TN, pp.235-241.

Blais, R.N., Copeland, G.E. and Lerner, T.H. 1975. Use of LARS system for the quantitative determination of smoke plume lateral diffusion coefficients from ERTS images of Virginia. As in Blais, 1974, v.IV, pp.621-633.

Bosanquet, C.H., Carey, W.F., and Halton, E.M. 1950. Dust deposition from chimney stacks. Proc. of the Inst. Mech. Engin. 162, 355-365.

Bowne, N.E. 1961. Some measurements of diffusion parameters from smoke plumes. Bull. Amer. meteor. Soc. 42, 2, 101-105.

Brimblecome, P., Armstrong, A. and Davies, T. 1978. Remote sensing of pollutant plumes from Landsat. J. Brit. Interplanet. Soc. 31,1,11-15.

Brimblecombe, P., and Davies, T.D. 1978. Detection of air pollution from Landsat-1. Weather 33, 1, 19-27.

Brown, R.M., Cohen, L.A., and Smith, M.E. 1972. Diffusion measurements in the 10-100 km range. J. of Appl. Meteor. 11,323-334.

Brown, F.R., Karn, F.S. 1976. Air pollution from the Ohio River and the Monongahela River valleys. In ERTS-1 - A new window on our planet, ed. by R.S.Williams, Jr, and W.D.Carter; Geological Survey professional paper 929. U.S.Govern. Print. Office, Washington, D.C., pp.261-265.

Carnegie, D.M. and Fine, B.T., 1977. Vegetation patterns. As in Barnes et. al., 1977, pp.256-257.

Clark, R.D.M. 1955. Photographic techniques for measuring diffusion parameters. 4th Atomic Energy Commission Air cleaning conference, Argonne Nat. Lab.; Tech. Inf. Serv. Extens. TID 7513(pt.I), 1956, pp.186-9.

Comtal 1980. Vision ONE/20 users manual. Comtal Corporation, Altadena, CA.

Conover, J..h. 1966. Anomalous cloud lines. J Atmos. Sci.23,6,778-785.

_____ 1969. New observations of anomalous cloud lines. J. Atmos. Sci.26,5,II,1153-4.

Copeland, G.E., Bandy, A.R., Kindle, E.C., Blais, R.N., and Hilton. G.M. 1973. Remote detection of aerolsol pollution by ERTS. Symp. on significant results obtained from the Earth Resources Technology Satellite-1, Goddard Space Flight Center, MD; NASA publication SP-327. U.S. Govern. Printing Office, pp.585-592.

Csanady, G.T. 1973. Turbulent diffusion in the environment. Dordrecht, Boston; D.Reidel Publ. Co.; pp.4-7.

Culkowski, W.M. 1961. Time exposure photography of smoke plumes. U.S.Atom. Energy Comm. Report ORO-359, Weather Bureau, Oak Ridge, Tenn.

Danielsen, E.F. 1981. Trajectories of the Mount St. Helens eruption plume. Science 211, 819-821.

Davies, E. LL., and Sutton, O.G. 1931. Some problems of modern meteorology, No.5 - the present position of the theory of turbulent motion in the atmosphere. Q. J. Roy. Met. Soc. 57,242,405-411.

Davies, R.W. 1959. Large-scale diffusion from an oil fire.
In Advances in Geophysics, vol. 6, ed. by F.N.Frenkiel
and P.A.Sheppard, Academic Press, New York: pp.413-415.

Einstein, A. 1905. On the movement of small particles
suspended in a stationary liquid demanded by the
molecular-kinetic theory of the Brownnian movement.
Translation publ. by Dover, New York., 1980(?), pp.1-
18; also notes by R.Furth, pp.86-104.

Ernst, J.A. 1975. A different perspective reveals air
pollution. Weatherwise,28,5,215-217.

Evans, Wn.E. 1974. Marking ERTS images with a small mirror
reflector. Photogrammetric Engineering 40,6,665-671.

Fick, A. 1855. On liquid diffusion. Phil. Mag., Ser.4, 10,
30-39.

Freden, S.C. 1976. Survey of the Landsat program. In
Mission to earth: Landsat views the world. ed. by
N.M.Short, P.D.Lowman Jr., S.C.Freden, and W.A.Finch
Jr.; NASA Publication S.P.-360. U.S. Govern. Printing
Office, Washington, D.C., pp.1-26 and 437-441.

Frenkiel, F.N. and Katz, . 1956. Studies of small-scale
turbulent diffusion in the atmosphere. J. Meteor. 13,
4, 388-394.

Friedman, J.D. and Heiken, G. 1977. Volcanoes and volcanic
landforms. As in Barnes et. al., 1977, pp. 137-147.

G.E. 1975. Image 100 user manual. Ground Systems
Department, Space Division, General Electric Company,
Daytona Beach, Fla.

Gifford, F.,Jr. 1955. Relative atmospheric diffusion of
smoke plumes. J. Meteor. 14, 5, 410-414.

_____ 1959. Smoke as quantitative air pollution indices.
Int. J. Air Poll. 2, 42-50.

_____ 1968. An outline of theories of diffusion in the lower
layers of the atmosphere. In Meteorology and Atomic
Energy, 1968, ed. by D.H.Slade; NTIS TDIS-24190; pp.65-
116.

_____ 1981. Smoke as a quantitative atmospheric diffusion
tracer. Atmospheric Environment 14,10,1119-1121.

Gifford, F.A., Hosker, R.P.Jr., and Rao, K.S. 1978.
Diffusion-deposition patterns in Martian streaks.
Icarus 36,133-146.

Gillani, N.V., Husar, R.B., Husar, J.D., and Patterson, D.E. 1978. Project MISTT: kinetics of particulate sulfur formation in a power plant plume out to 300 km. Atmospheric Environment 12,589-598.

Gird, r. 1982. Personal communication about his work at the National Oceanic and Atmospheric Administration - NOAA, Camp Springs, MD.

Grigoryev, Al.A., and Lipatov, V.B. 1975. Space remote sensing of smokes. As in Barringer and Davies, 10th symp., v.I, pp. 305-318.

Halitsky, J. 1961. Single-camera measurements of smoke plumes. Int.J.Air and Water Poll. 4,3/4,185-198.

Halitsky, J., Randell, C.P., and Hackman,I.M. 1950. Communications (on Dust deposition from chimney stacks, by Bosanquet et.al., 1950). Proc. of the Inst. Mech. Engin. 162,p.366 and 4 plates.

Henry, V. 1908. Comptes Rendus,146,1024, and 147,62.

Hilst, G.R. 1957. The dispersion of stack gases in stable atmospheres. J.Air Poll.Cont.Assoc. 7,3,205-210.

Hilton, G.M., and Blais, R.N. 1974. Determination of physical parameters of smoke from aerial photography for input to computer plume models. As in Blais, 1974, pp. 243-251.

Hogstrom, U. 1964. An experimental study on atmospheric diffusion. Tellus 16,2,205-251.

Holz, B.K. 1977. Cultural features imaged and observed from Skylab 4. As in Barnes et. al., pp.236, 238-239.

Hoult, D.P., Fay, J.A., and Forney, L.J. 1969. A theory of plume rise compared with field observations. J. Air Poll. Control Assoc. 19,8,585-590.

INPE 1973-9. Landsat archives. "Instituto de Pesquisas Espaciais", Sao Jose dos Campos e Cachoeira Paulista, S.P., Brazil.

Islitzer, N.F. and Slade, D.H. 1968. Diffusion and transport experiments. In Meteorology and atomic energy, 1968, ed. by D.H.Slade; U.S.Atom. Energy Comm.; NTIS/TID-24190; pp.117-188(pg.152).

Jacko, R.B., Neuendorf, D.W., and Blandford, J.R. 1978.
Plume parameters and particulate emissions from the by-
product coke oven pushing operation. Air Pollution
Control Association, 71st. Annual meeting, Houston,
Texas; paper 78-9.4., 14 pp.

Jagger, G. 1982. As in Gird, 1982.

Keafer, L.S., Kopia, P. 1973. Development of flight
experiments for remote measurement of pollution. As in
Blais, 1974, v.II, pp.129-163.

Kellog, W.W. 1956. Diffusion of smoke in the stratosphere.
J. Meteor. 13,3,241-250.

Klauber, G. 1973. Ultraviolet photography of sulfur
dioside. Environ. Sci. Technol. 7,10,953-954.

LARS 1973. LARSYS users manual. Laboratory for
Applications of Remote Sensing, Purdue University, West
Lafayette, IN. 3 volumes.

LARS 1977. Remote sensing of agriculture, earth resources
and man's environment. Laboratory for Applications of
Remote Sensing, Purdue University, West Lafayette, IN,
32 pp.;see pg.11.

LARS 1980. LARSFRIS user's manual. Laboratory for
Applications of Remote Sensing, Purdue University, West
Lafayette, IN. 4 vols.

LaBastille, A., and Spiegel, T. 1981. Acid rain - How great
a menace? Geographic Magazine 160,5(nov.),652-681.

Larsen, P. 1970. Photographic techniques applicable to
earth resources analyses. U.S.NASA Technical Memorandum
TM X-64546.

Ludwig, C.B., Griggs, M., Malkus, W., and Bartle, E.R. 1974.
Measurement of air pollutants from satellites; 1:
feasibility considerations. Appl. Opt. 16,6,1494-1509.

Lyons, W.A. 1973. The use of ERTS imagery in air pollution
and mesometeorological studies around the Great Lakes.
3rd earth Resources Technology Satellite-1 Symposium,
v.I, sect.B. U.S.NASA publ. SP-351. U.S.Govrenm.
Printing Off., pp.1491-1504.

_____ 1975. Turbulent diffusion and pollutant transport in
shoreline environments. In Lectures on air pollution
and environmental impact analyses, Amer. Meteor. Soc.,
Boston, Mass., pp.136-208.

Lyons, W.A. 1974. Satellite detection of air pollutants. Proceed., Symp. on Remote sensing applied to energy related problems, ed. by T.N.Vaziroglu, John Wiley & Sons, New York, 1975. pp.263-290.

Lyons, W.A., Dooley, J.C.Jr, and Whitby, K.T. 1978. Satellite detection of long-range pollution transport and sulfate aerosol hazes. Atmospheric Environment 12,621-631.

Lyons, W.A. and Husar, R.B. 1976. SMS/GOES visible images detect a synoptic/scale air pollution episode. Month. Weath. Rev. 104,12,1623-1626.

Lyons W.A., and Pease, S.R. 1973. Detection of particulate air pollution plumes from major point sources using ERTS-1 imagery. Bull. Amer. meteor. Soc. 54,11,1163-1170.

Lyons, W.A., and Pease, S.R. 1973a. ERTS-1 views the Great Lakes. As Copeland et. al., 1973, pp.847-854.

Lyons, W.A., Keen, C.s., and Northouse, R.A. 1974. ERTS-1 satellite observations of mesoscale air pollution dispersion around the Great Lakes. Symp on atmospheric diffusion and air pollution, Santa Barbara, CA; Amer. Meteor. Soc., Boston, Mass., pp.273-280.

M.A. 19773-8. Meteorological data from the "Estacao Alcalis, Cabo Frio", lat.22°59'S and long.42°02'W, "Ministerio da Agricultura", Brazil.

Maslowski, A. 1981. Mining a meteor crater. Astronomy 9,4,18-22. 9,4,18-22.

McKee, E. D., Breed, C.S., and Fryberger, S. 1977. Desert sand seas. As in Barnes et. al., 1977, pp.41-43.

MacLead, N.H., Schubert J.S., and Anaejionu 1977. Report on the Skylab-4 african drought and arid land experiment. As in Barnes et. al., 1977, pp.263-286.

McLellan, A. 1971. Satellite remote sensing of large scale local atmospheric pollution. Proc. 2nd. Int. Clean Air Congr., ed. by H.M.Englund and W.T.Berrry. Academic press, pp. 570-575.

_____ 1971. Atmospheric pollution detection by satellite remote sensing. As in Barringer and Davies, 1978; 7th Symp., v.I, pp.563-584.

Matson, M., and Staggs, S.J. 1981. The Mt. St. Helens ash cloud. Bull. Amer. meteor. Soc. 62,10,1486.

Matson, M. 1982. As in Gird, 1982.

Millan, M.M. 1976. A note on the geometry of plume diffusion measurements. Atmospheric Environment 10,655-252.

Millan, M.M., and Chung, Y.S. 1977. Detection of a plume 400 km from the source. Atmospheric Environment 11,939-944.

Monin, A.S. 1969. Smoke propagation in the surface layer of the atmosphere. As in Davies, 1969, pp.331-343.

Moore, C.B., Smith, J.R., and Gaalswyk, A. 1954. On the use of constant-level balloons to measure horizontal motions in the atmosphere. J.Meteor. 11,3,167-172.

Morabito, L.A., Synnott, S.P., and Collins, S.A. 1979. Discovery of currently active extraterrestrial volcanism. Science 204,972.

Murtha, P.A. 1973. SO_2 damage to forests recorded by ERTS-1. As in Lyons, 1973, pp.137-143.

Murtha, P.A. 1973a. ERTS records SO_2 fume damage to forests, Wawa, Ontario. For. Chron. 49,6,251-252.

Nappo, C.J.Jr. 1978. Relative and single particle diffusion estimates determined from smoke plume photographs. Preprints, 4th Symp. Turbul., diff. and air pollut., Amer. Meteor. Soc., Boston, MA. pp.46-47.

_____ 1981. Atmospheric turbulence and diffusion estimates derived from observations of a smoke plume. Atmospheric Environment 15,4,541-547.

NASA 1971. Remote measurement of pollution. U.S.NASA publication SP-285. U.S.Governm. Print. Office, Washington, D.C., 235pp.

_____ 1976. Landsat-data users handbook. U.S.NASA document No. 76 sds 4258; U.S.Govern. Printing Off., Washington, D.C.

_____ 1977. NASA facts: Landsat (a poster). U.S.Govern. Print. Office, Wawshington, D.C. (stock No.033-000-00702-7)

Nijland, J.A. 1979. Characteristics of air pollution plumes observed from Landsat satellites. S. Afr. J. of Sci. 75,311-313.

Nelson, C.N. and Hamsher, D.H. 1950. Photogrtaphy of high altitude objects. J. Opt. Soc Am. 40,12,863-875.

Nonhebel, G. 1960. Recommendations on heights for new industrial chimneys. J. Inst. Fuel 33,479-511.

Pasquill, F. 1961. The estimation of the dispersion of windborne material. Met. Mag. 90,1063,33-49.

Pease, R.W, and Bowden, L.W. 1969. Making color infrared film a more effective high-altitude remote sensor. Rem. Sens. of Environ. 1,23-30.

Pettyjohn, W.A. 1980. Environmental geoscience. In Remote sensing in geology, ed. by B.S.Siegel and A.R.Gillespie; New York, John Willey; pp.641-657.

Pettyjohn, W.A. and McKeon, J.B. 1976. Satellite detection of smoke plumes and inadvertent weather modification. In Proceed., Symp. on acid precipitation and the forest ecosystem; USDA Forest Service Gen. Tech. Rept. NE-23, pp.337-347.

Prospero, J.M., Bonatti, E., Shubert, C., and Carlson, T.N. 1970. Dust in the Caribbean atmosphere traced to an african dust storm. Earth Planet. Sci. Letters 9,3,287-293.

Randerson, D. 1968. A study of air pollution sources as viewed by earth satellites. J. Air Poll. Control Assoc. 18,4,249-253.

_____ 1977. Quantitative analysis of atmospheric pollution phenomena. As in Barnes et al., 1977, pp.381-405.

Randerson, D., Garcia, J.G., and Whitehead, V.S. 1971. Photogrammetric and photometric investigation of a smoke plume viewed from space. J.of Appl. Meteor 10,1122-1131.

Raynor, G.S., Michael, P., Brown, R.W., and Sethuraman, S 1974. A research program on atmospheric diffusion from an oceanic site. As in Lyons et al., 1974, pp.273-280.

Reynolds, O. 1883. An experimental investigation of the circumstances which determine whether the motion of water shall be direct or sinuous, and of the law of resistance in parallel channels. Phil. Trans. Roy. Soc. London 174-III,935-982.

Richardson, L.J. 1920. Some measurements of atmospheric turbulence. Phil. Trans. Roy. Soc. London Ser. A,221,1-28.

Richardson, L.J. 1926. Atmospheric diffusion shown on a distance-neighbour graph. Proc. Roy. Soc. A-110,709-737.

_____ 1929. A search for the law of atmospheric diffusion. Beitr. Phys. frei Atmos. 15,24-29.

Richardson, L.F. and Proctor, d. 1925. Diffusion over distances ranging from 3 km to 86 km. Mem. Roy. Met. Soc. 1,1,1-16.

Roberts, O.F.T. 1923. The theoretical scattering of smoke in a turbulent atmosphere. Proc. Roy. Soc. A-104,640-654.

Rosenfeld, C.L. 1980. Observations on the Mount St.Helens eruption. Sci. Am. 68,5,494-509.

Saissac, J. 1958. "Sur la diffusion atmospherique des particules." Com. Rend. 247,17,1371-1374.

Sartor, J.D., Katz, I., and Katz, R.E. 1952. A mobile method for measuring atmospheric diffusion. Bull. Amer. meteor. Soc. 33,5,188-194.

Schaefer, V.J. and Day, J.A. 1891. A field guide to the atmosphere. Hoghton Mifflin Co., Boston; pg.34.

Scorer, R.S. 1959. The behavior of chimney plumes. Int. J. Air Poll. 1,198-220.

_____ 1978. Environmental Aerodynamics; Ellis Horwood, Chichester, pp.360-362.

Seddig 1908. Phys. Zeit.9,465 and Zeit. f. Elektrochem,73,360(1912).

Setzer, A. 1981. Study of a 150 km long plume using Landsat imagery. Preprints, 5th Symp. on Turbulence, diffusion and air pollution, Amer. Meteor. Soc., Boston, Mass, pp.46-47.

Setzer, A.W. and Molion, L.C.B. 1979. "the use of remote sensing in the study of atmospheric pollution dispersion" (in portuguese). Presented at the 31st meeting of the Brazilian Society for the Advancement of Science-"SBPC".

Setzer, A.W., Jacko, R.B., and Hoffer,R.M. 1982. The use of color-IR photos for air pollution plumes. J. Air Poll Control Assoc. 32,8,837-838.

Short, N.M., Lowman, P.D., Freden, S.C., and Fincls, W.A. 1976. Mission to earth: Landsat views the world. U.S.NASA, publication SP-380; U.S.Governm. Printing Office,Washington,D.C.; pp.73,96,181,205,285,311,357,433.

Smith, B.A. et al. 1979. The Jupiter system through the eyes of voyager 1. Science 204,951-972.

Snyder, J.F., Ashman, J.P. and Brandli, H.W. 1976. Meteorological satellite coverage of Florida Everglades fires. Mont. Weath. Rev. 104,10,1330-1332.

Staylor, W.F. 1978. Determination of stack properties from satellite imagery. J. Spacecr. Rockets 15,2,92-99.

Stevenson, R.E., Carter, D.L., VonderHaar, S.P., and Stone, R.O. 1977. Visual observations of the ocean. As in Barnes et al.,1977; pp.306-307.

Sutton, O.G. 1932. A theory of eddy diffusion in the atmosphere. Proc. Roy. Soc. A-135,143-165.

Taylor, G.I. 1915. Eddy motion in the atmosphere. Phil. Trans. Roy. Soc. London A-215,1-26.

Tempelmeyer, K.E., and Ey, D. 1974. Use of remote sensing to study the dispersion of stack plumes. As in Blais, 1974, pp.255-272.

Thomson, D.W. 1975. ACDAR meteorology: the application and interpretation of atmospheric acoustic sounding measurements. 3rd. Symp. on meteorological observations and instrumentation, Amer. Meteor. Soc., Boston, Mass., pp.144-150.

Torbert, G. 1976. Monitoring forest-fire burn areas in Alaska. As in Brown and Karn, 1976, pp.244-245.

Torsani, J.A. 1981. "Applications of remote sensing in the study of atmospheric pollution diffusion". MSc thesis, Instituto de Pesquisas Espaciais, S.J. dos Campos, S.P., Brazil; INPE-2192-TDL/059 (in portuguese). 106 pp.

Turner, D.B. 1969. Workbook of atmospheric dispersion estimates. U.S.Depart. of Health, Education and Welfare; Public Health Service Publication No. 999-ap-26.

U.N. 1969. Chemical and bacteriological (biological) weapons and the effects of their possible use. United Nations Report No.E.69.I24, New york.

Underwood, R.W., 1968. Color photography from space. As in Anson, 1968, pg.376.

Utha, E.E. and Wilson, W.E., 1981. Lidar observations of the density of the Labadie power plant plume. Atmospheric Environment 13,10,1395-1412.

Veress, S.A. 1970. Air pollution research. Photogrammetric engineering 36,8,840-848.

_____ 1970a. Study of three-dimensional extension of polluted air. Univ. of Washington, Depart. of Civil Engin.

_____ 1972. Extintion coefficient. Photogrammetric Engineering 38,2,183-191.

Vermillion, C.H. 1977. NOAA-5 views dust storm. Bull. Am. met. Soc. 58,4,330.

Vinogradov, B.V., Grigoryev, A.A., and Lipatov, V.B. 1972. Structure of dust storms from ITOS-I T.V. images obtained over Iraq and the Gulf of Persia. as in Barringer and Davies, 1978, 8th. Symposium; pp.463-466.

Whitaker, R. and Hilst, G. 1981. Mapping air quality by Laser. EPRI Journal, Jul./Aug. 1981,15-20.

Wightman, J.M. 1973. Detection, mapping and estimation of spread of grass fires from Southern African ERTS-1 imagery. As in Copeland et al., pp.593-601.

Withington, C.F. 1976. Oil-well fire on ERTS-1 images. As in Rown and Karn, 1976; pp.258-260.

Wobber, F.J. 1969. Environmental studies using earth orbital photography. Photogrammetria 24,107-165.

_____ 1970. Orbital photos applied to the environment. Photogrammetric Engineering 36,8,852-864.

Woodcock, A.H. and Wyman, J. 1947. Convective motion in air over the sea. Ann. N.Y. Acad. Sci. 48,749-777.

APPENDIX

Average emission data for the air pollution sources whose plumes can be seen on Figures 4.1 to 4.18 were obtained from the National Emission Data System (Point Source Listing, Lake County, IN), prepared by the U.S.Environmental Protection Agency. The following pages were copied from the listing of the Air Pollution Laboratory, School of Civil Engineering, Purdue University. The emission rates and source data should be regarded only as a rough indication of the real situation when the images were obtained. Industrial operations are subject to normal temporal variations of the processes and units and also of the raw materials. Also, the plumes probably originated from many sources so close that the Landsat sensors could not separate them. The following emissions represent the strongest individual sources in each industrial complex. The long plume that originates at the lowe-left corner of Figure 4.2 is from a steel complex (pages 126 and 127). Following the shoreline to the right, the small plume is probably from a cement plant (page 128), although it could also be associated with a power plant (page 129) because the two sources are vrey close. The third (long) plume is either from a steel complex (pages 130 and 131) and/or from another cement plant (page 132) since these two sources are along the plume axis. The total particulate emissions for the regions of origin of these three plumes was also evaluated by Lyons and Pease (1973) as 84,474, 144,627, and 88,597 tons/year, respectively.

126

FILE CREATED ON WEDNESDAY   JULY 20, 1977   PAGE 297
NATIONAL EMISSION DATA SYSTEM
POINT SOURCE LISTING

STATE(17): INDIANA   AQCR(067): METROPOLITAN CHICAGO   CITY(1180): EAST CHICAGO
COUNTY(23801): LAKE CO   PLANT ID: 0015 POINT ID: 62

NAME-ADDRESS: INLAND STEEL, 3210 WATLING ST PART A   SIC(3312): BLAST FURNACES (INCLUDING COKE OVEN), STEEL WORKS & ROLLING MILL
PERSONAL CONTACT: BROUGH J   SCC(3-03-009-03): INDUSTRIAL PROCES -PRIMARY METALS   -STEEL PRODUCTION -BOF-GENERAL

GENERAL INFORMATION   UTM GRID COORDINATES   HAND CALCULATED POINT EMISSIONS   ALLOWABLE EMISSIONS FOR POINT
DATE 3P   UTM ZONE: 16   PARTICULATE: PARTICULATE: 297 TONS/YR
LAST UPDATE: 1974   SOX: 1,000 TONS/YR   SOX: 0 TONS/YR
OWNERSHIP: PRIVATE   HORIZONTAL: 461.0 KM   NOX: 0 TONS/YR   NOX: 0 TONS/YR
                             VERTICAL: 4,612.0 KM   HC: 0 TONS/YR   HC: 0 TONS/YR
IPP PROCESS: 02   CO: 289,000 TONS/YR   CO: 0 TONS/YR

SOURCE: PROCESS   STACK PARAMETERS   EMISSION ESTIMATION METHODS   COMPUTER CALCD SCC EMISSIONS
                             STACK HEIGHT: 140 FT   PART: NADB-APPROVED NON-EPA EMIS FACTOR   PART: 1,040 TONS/YR
                             STACK DIAMETER: 13.0 FT   SOX: EMISSION FACTOR(AP-42 OR PENDING)
NORMAL OPERATIONS   GAS TEMPERATURE: F   NOX: EMISSION FACTOR(AP-42 OR PENDING)   SOX: TONS/YR
                             GAS FLOW RATE: ACFM   HC: EMISSION FACTOR(AP-42 OR PENDING)
HOURS/DAY: 24   PLUME HT/NO STACK: 0   FT   CO: EMISSION FACTOR(AP-42 OR PENDING)   NOX: TONS/YR
DAYS/WEEK: 7   SAME STACK W/THIS POINTS
WEEKS/YEAR: 52   HC: TONS/YR
                             CONTROL DEVICE/METHOD IDENTIFICATION   CONTROL
                             PRIMARY PART: WET SCRUBBER - HIGH EFFICIENCY EFFICIENCIES   CO: 289,000 TONS/YR
ANNUAL THROUGHPUT   SECOND. PART: NO CONTROL EQUIPMENT   PART: 99.0 %
   DEC-FEB: 25 %
   MAR-MAY: 25 %   PRIMARY SOX: NO CONTROL EQUIPMENT   SOX: 00.0 %
   JUNE-AUG: 25 %   SECOND. SOX: NO CONTROL EQUIPMENT
   SEPT-NOV: 25 %
                             PRIMARY NOX: NO CONTROL EQUIPMENT   NOX: 00.0 %
SPACE HEAT: 00.0 %   SECOND. NOX: NO CONTROL EQUIPMENT

COMPLIANCE INFO   PRIMARY HC: NO CONTROL EQUIPMENT   HC: 00.0 %
                            SECOND. HC: NO CONTROL EQUIPMENT
NOT SPECIFIED
                             PRIMARY CO: NO CONTROL EQUIPMENT   CO: 00.0 %
SCHEDULE   /   SECOND. CO: NO CONTROL EQUIPMENT
COMPLIANCE DATE: /
                             FUEL CHARACTERISTICS   OPERATING RATES
COMPLIANCE STATUS   ANNUAL OPERATING RATE: 4,030,000 TONS PRODUCED
UPDATE: / /   FUEL SULFUR CONTENT: 0.00 % HOURLY MAXM DESIGN RATE: 457,650 TONS PRODUCED
EMERGENCY CONTROL
ACTION PLAN   FUEL ASH CONTENT: 00.0 %   BOILER DESIGN CAPACITY:
STATUS: UNKNOWN
                             FUEL HEAT CONTENT: COMMENTS: NO 4 BOF STCK 3B

127

FILE CREATED BY WEDNESDAY --- JULY 20, 1977
NATIONAL EMISSIONS DATA SYSTEM
PAGE 215

POINT SOURCE LISTING

STATE CITY: INDIANA
COUNTY: 36C11 LAKE CO
AGENCY 6671: METROPOLITAN CHICAGO
PLANT ID: 0015 POINT IC: 10
CITY 11801: EAST CHICAGO

NAME-ADDRESS: INLAND STEEL 3210 WATLING ST PART A   SIC 3312: BLAST FURNACES (INCLUDING COKE OVEN), STEEL WORKS & ROLLING MILL
PERSONAL CONTACT: BROUGH J   SCC 13-90-007-39: INDUSTRIAL PROCES -THPROCESS FUEL   -PROCESS GAS   -OTHER/NOT CLASSIFIED

GENERAL INFORMATION   HAND CALCULATED POINT EMISSIONS   ALLOWABLE EMISSIONS FOR POINT

UTM GRID COORDINATES
UTM ZONE: 16

	PARTICULATE:			PARTICULATE:	
	SOX:	1,330 TONS/YR		SOX:	1,660 TONS/YR
	NOX:	0 TONS/YR		NOX:	0 TONS/YR
	HC:	0 TONS/YR		HC:	0 TONS/YR
	CO:	0 TONS/YR		CO:	0 TONS/YR

DATE OF
LAST UPDATE: 1974

OWNERSHIP: PRIVATE

HORIZONTAL: 463.0 KM
VERTICAL: 4,612.0 KM

TPP PROCESS: 04

STACK PARAMETERS

COMPUTER CALCD SCC EMISSIONS

EMISSION ESTIMATION METHODS

	PART:		TONS/YR
	SOX:	1,330	TONS/YR
	NOX:		TONS/YR
	HC:		TONS/YR
	CO:		TONS/YR

SOURCE: COMBUSTION
STACK HEIGHT: 250 FT
STACK DIAMETER: 11.0 FT
GAS TEMPERATURE: 565 F

PART: NOT APPLICABLE
SOX: MATERIAL BALANCE & ENGR KNOWLEDGE
NOX: NOT APPLICABLE
HC: NOT APPLICABLE
CO: NOT APPLICABLE

NORMAL OPERATIONS
GAS FLOW RATE: 339,250 ACFM
PLUME HEIGHT/NO STACK: 0 FT
SAME STACK NEMIS POINTS

HOURS/DAY: 24
DAYS/WEEK: 7
WEEKS/YEAR: 52

CONTROL DEVICE/METHOD IDENTIFICATION

	CONTROL EFFICIENCIES	
PRIMARY PART: NO CONTROL EQUIPMENT SECOND. PART: NO CONTROL EQUIPMENT	PART: 00.0 %	
PRIMARY SOX: NO CONTROL EQUIPMENT SECOND. SOX: NO CONTROL EQUIPMENT	SOX: 00.0 %	
PRIMARY NOX: NO CONTROL EQUIPMENT SECOND. NOX: NO CONTROL EQUIPMENT	NOX: 00.0 %	
PRIMARY HC: NO CONTROL EQUIPMENT SECOND. HC: NO CONTROL EQUIPMENT	HC: 00.0 %	
PRIMARY CO: NO CONTROL EQUIPMENT SECOND. CO: NO CONTROL EQUIPMENT	CO: 00.0 %	

ANNUAL THROUGHPUT
DEC-FEB: 25 %
MAR-MAY: 25 %
JUNE-AUG: 25 %
SEPT-NOV: 25 %

SPACE HEAT:

COMPLIANCE STATUS
UPDATE: / /

COMPLIANCE TYPE
NOT SPECIFIED

FUEL CHARACTERISTICS

OPERATING RATES

ANNUAL OPERATING RATE: 2,050 MILLION CUBIC FEET BURNED

HOURLY MAX H DESIGN RATE: .335 MILLION CUBIC FEET BURNED

FUEL SULFUR CONTENT: 1.50 %

SCHEDULED
COMPLNCE DATE: / /

EMERGENCY CONTROL
ACTION PLAN

FUEL ASH CONTENT: 00.0 %

BOILER DESIGN CAPACITY: 221 MILLION BTU/HR

STATUS UNKNOWN

FUEL HEAT CONTENT: 540 MILLION BTU/MILLION CUBIC FEET BURNED   COMMENTS: BATT NO 2 COKE GAS

PAGE 420

FILE CREATED ON WEDNESDAY   JULY 20, 1977

NATIONAL EMISSIONS DATA SYSTEM

POINT SOURCE LISTING

STATE(15): INDIANA   AQCR(067): METROPOLITAN CHICAGO   CITY(152C): GARY
COUNTY(23601): LAKE CO
PLANT ID: C032   POINT ID: 03
NAME-ADDRESS: 6 N MITCHELL STA NIPSCO CLARK RD & LK MI SIC(4911): (ELECTRIC) SERVICES
PERSONAL CONTACT: F PANN   SCC(1-01-002-02): EXTERNAL COMB BOILER -ELECTRIC GENERATN -BITUMINOUS COAL -STOKER/PULVDRY

GENERAL INFORMATION	UTM GRID COORDINATES	HAND CALCULATED POINT EMISSIONS	ALLOWABLE EMISSIONS FOR POINT
	UTM ZONE: 16	PARTICULATE:	PARTICULATE: 586 TONS/YR
DATE OF LAST UPDATE: 1977		SOX: 11,500 TONS/YR	NOX: 1,750 TONS/YR
	HORIZONTAL: 466.1 KM	NOX: 3,460 TONS/YR	NOX: 0 TONS/YR
OWNERSHIP: UTILITY	VERTICAL: 4,609.5 KM	HC: 56 TONS/YR	HC: 0 TONS/YR
		CO: 189 TONS/YR	CO: 0 TONS/YR

	STACK PARAMETERS	EMISSION ESTIMATION METHODS	COMPUTER CALCD SCC EMISSIONS
IPP PROCESS: 20	STACK HEIGHT: 236 FT	PART: EMISSION FACTOR(AP-42 OR PENDING)	PART: 1,150 TONS/YR
SOURCE: BOILER	STACK DIAMETER: 11.3 FT	SOX: EMISSION FACTOR(AP-42 OR PENDING)	
	GAS TEMPERATURE: 290 F	NOX: EMISSION FACTOR(AP-42 OR PENDING)	SOX: 11,500 TONS/YR
NORMAL OPERATIONS	GAS FLOW RATE: 820,000 ACFM	HC: EMISSION FACTOR(AP-42 OR PENDING)	
	PLUME HT (NO STACK): 0 FT	CO: EMISSION FACTOR(AP-42 OR PENDING)	NOX: 3,390 TONS/YR
HOURS/DAY: 24	SAME STACK VENTS POINTS 03-04		
DAYS/WEEK: 7			HC: 56 TONS/YR
WEEKS/YEAR: 52	CONTROL DEVICE/METHOD IDENTIFICATION	CONTROL EFFICIENCIES	
	PRIMARY PART: ELECTROSTATIC PRECIPITOR - HIGH EFFIC	PART: 96.0 %	CO: 186 TONS/YR
% ANNUAL THROUGHPUT	SECOND. PART: NO CONTROL EQUIPMENT		
DEC-FEB: 25 %	PRIMARY SOX: NO CONTROL EQUIPMENT	SOX: 00.0 %	
MAR-MAY: 27 %	SECOND. SOX: NO CONTROL EQUIPMENT		
JUNE-AUG: 27 %	PRIMARY NOX: NO CONTROL EQUIPMENT	NOX: 00.0 %	
SEPT-NOV: 20 %	SECOND. NOX: NO CONTROL EQUIPMENT		
% SPACE HEAT: 00.1 %	PRIMARY HC: NO CONTROL EQUIPMENT	HC: 00.0 %	
	SECOND. HC: NO CONTROL EQUIPMENT		
COMPLIANCE INFO	PRIMARY CO: NO CONTROL EQUIPMENT	CO: 00.0 %	
NOT SPECIFIED	SECOND. CO: NO CONTROL EQUIPMENT		
SCHEDULED			
COMPLNCE DATE: / /	FUEL CHARACTERISTICS	OPERATING RATES	
COMPLIANCE STATUS		ANNUAL OPERATING RATE: 311,030 TONS BURNED	
UPDATE: / /	FUEL SULFUR CONTENT: 1.65 %	HOURLY MAX'M DESIGN RATE: 42,350 TONS BURNED	
ENFORCEMENT CONTROL ACTION PLAN	FUEL ASH CONTENT: 09.1 %	BOILER DESIGN CAPACITY: 1,250 MILLION BTU/HR	
STATUS UNKNOWN	FUEL HEAT CONTENT: 21 MILLION BTU/TONS BURNED	COMMENTS: UNIT NO 6	

STATE: INDIANA   AGENCY: METROPOLITAN CHICAGO   CITY/SIZE: GARY
COUNTY: LAKE CO   PLANT ID: 0002   POINT ID: 02

NAME/ADDRESS: UNIV ATLAS CEMENT BUFFINGTON STA 46901   SIC(22)I: CEMENT, HYDRAULIC
PERSONAL CONTACT: R TORONG   SCC(1-2S-C6-C5): INDUSTRIAL PROCESS   -MINERAL PRODUCTS   -CEMENT MFG DRY   -KILNS-COAL FIRED

GENERAL INFORMATION	UTM GRID COORDINATES	HAND CALCULATED POINT EMISSIONS	ALLOWABLE EMISSIONS FOR POINT
		PARTICULATE: 3,500 TONS/YR	PARTICULATE: 84 TONS/YR
DATE OF	UTM ZONE: 16	SOX: 5,130 TONS/YR	SOX: 0 TONS/YR
LAST UPDATE: 1973	HORIZONTAL: 470.0 KM	NOX: 0 TONS/YR	NOX: 0 TONS/YR
	VERTICAL: 4,607.0 KM	HC: 0 TONS/YR	HC: 0 TONS/YR
OWNERSHIP: PRIVATE		CO: 0 TONS/YR	CO: 0 TONS/YR

IPP PROCESS: 01	STACK PARAMETERS	EMISSION ESTIMATION METHODS	COMPUTER CALCO SCC EMISSIONS
SOURCE: PROCESS	STACK HEIGHT: 103 FT	PART: FACIL. CLOSED, OPERA. CEASED	PART: TONS/YR
	STACK DIAMETER: 8.0 FT	SOX: FACIL. CLOSED, OPERA. CEASED	
NORMAL OPERATIONS	GAS TEMPERATURE: 400 F	NOX: FACIL. CLOSED, OPERA. CEASED	SOX: TONS/YR
	GAS FLOW RATE: 53,217 ACFM	HC: FACIL. CLOSED, OPERA. CEASED	
HOURS/DAY: 24	PLUME HT/NO STACK: 0 FT	CO: FACIL. CLOSED, OPERA. CEASED	NOX: TONS/YR
DAYS/WEEK: 7	SAME STACK VENTS POINTS		
WEEKS/YEAR: 52		CONTROL	HC: TONS/YR
	CONTROL DEVICE/METHOD IDENTIFICATION	EFFICIENCIES	
ANNUAL THROUGHPUT	PRIMARY PART: ELECTROSTATIC PRECIPITOR - HIGH EFFIC	PART: 97.0 %	CO: TONS/YR
	SECOND. PART: NO CONTROL EQUIPMENT		
DEC-FEB: 25 %			
MAR-MAY: 25 %	PRIMARY SOX: NO CONTROL EQUIPMENT	SOX: 00.0 %	
JUNE-AUG: 25 %	SECOND. SOX: NO CONTROL EQUIPMENT		
SEPT-NOV: 25 %			
	PRIMARY NOX: NO CONTROL EQUIPMENT	NOX: 00.0 %	
% STACK HEAT: 60.0 %	SECOND. NOX: NO CONTROL EQUIPMENT		
	PRIMARY HC: NO CONTROL EQUIPMENT	HC: 00.0 %	
COMPLIANCE INFO	SECOND. HC: NO CONTROL EQUIPMENT		
NOT SPECIFIED			
	PRIMARY CO: NO CONTROL EQUIPMENT	CO: 00.0 %	
SCHEDULED	SECOND. CO: NO CONTROL EQUIPMENT		
COMPLIANCE DATE: /			
	FUEL CHARACTERISTICS	OPERATING RATES	
COMPLIANCE STATUS: /			
UPDATE: /	FUEL SULFUR CONTENT: 0.00 %	ANNUAL OPERATING RATE: 484,000 TONS CEMENT PRODUCED	
EMERGENCY CONTROL		HOURLY MAXIMUM DESIGN RATE:	
ACTION PLAN	FUEL ASH CONTENT: 00.0 %	BOILER DESIGN CAPACITY:	
STATUS UNKNOWN			
	FUEL HEAT CONTENT:	COMMENTS: CLINKER PRODUCTION	

VITA

VITA

Mr. Alberto W. Setzer was born in the city of Sao Paulo, S.P., Brazil, on March/14/1951.

He obtained his degree in Mechanical Engineering on Dec./ 73 from "Escola de Engenharia Maua", S.C. do Sul, S.P., Brazil. The degree of MSc in Environmental Engineering (field of Air Pollution) was obtained on Aug./77 at the Technion Institute of Technology, Haifa, Israel.

On Aug./79, with a grant from the Brazilian government ("CNPq"), he came to the School of Civil Engineering of Purdue University, West Lafayette, IN, for a PhD program in Environmental Engineering (field of Air Pollution).

Mr. Setzer has a teaching experience of four years and also worked for different engineering companies. He also spent two years at "INPE", S.J. dos Campos, S.P., Brazil (the Brazilian Space Research Institute) where he was involved with the uses of satellites in environmental problems.